INSTITUTE OF PHYSICS PUBLISHING REPORTS ON PROGRESS IN PHYSICS

Rep. Prog. Phys. **64** (2001) 1657–1701 PII: S0034-4885(01)08170-2

Nuclear reactions and stellar processes

K Langanke[1] **and M Wiescher**[2]

[1] Institute for Physics and Astronomy, University of Aarhus, DK-8000 Aarhus C, Denmark
[2] Department of Physics, University of Notre Dame, IN 46556, USA

Received 6 July 2001, in final form 30 August 2001
Published 7 November 2001
Online at stacks.iop.org/RoPP/64/1657

Abstract

Nuclear Astrophysics is concerned with the study of nuclear processes at stellar temperature and density conditions. A main goal is the understanding of the synthesis of the elements and the generation of energy guiding stellar evolution and driving stellar explosions. Observables (like e.g. luminosity curves or elemental abundance distributions) witness the interplay between nuclear structure aspects near the particle drip-lines and the appropriate astrophysical environments, and give guidance to and constraints on stellar conditions and the associated nucleosynthesis. We present an overview of the broad range of nucleosynthesis scenarios from the Big Bang to the different conditions during stellar evolution and stellar explosion. Special emphasis is given to the discussion of nuclear physics aspects of pre-supernova collapse and supernova shock front nucleosynthesis. Of great interests are presently nucleosynthesis processes far from the limits of stability like the neutron diriven r-process and the hydrogen driven rp-process. The nuclear physics of the r-process and the possible site for the r-process in the neutrino driven wind of the supernova shock are discussed and the possible impact of neutrino induced processes is presented. Hydrogen induced explosive processes occur in the thermonuclear runaway on the surface of accreting compact stars at electron degenerate conditions. This includes novae triggered by accretion on white dwarfs and x-ray bursts initiated by accretion on neutron stars. High accretion rates on white dwarfs and neutron stars lead to supernova type Ia explosions or to x-ray pulsars respectively. An overview of the nucleosynthesis conditions and uncertainties is given for all of these scenarios.

(Some figures in this article are in colour only in the electronic version)

Contents

1. Introduction

Astronomical observations of luminosities and spectra of galaxies, stars, nova and supernova explosions as well as the interstellar and intergalactic medium give evidence for the nuclear processes driving stellar evolution and stellar explosion. In recent years, however, observations which detect particles, such as neutrinos, high-energy cosmic rays and gamma-rays, as well as the chemical and physical analysis of meteoritic dust material, have also gained importance as new analytical tools for observation and have added new insight for the understanding of the nuclear processes driving stellar evolution and stellar explosion and responsible for the origin of the observed elements in our universe. Abundances of elements/nuclei serve as signatures for nucleosynthesis processes in a wide range of stellar scenarios; they are determined from the analysis of radio lines of interstellar matter, quasar absorption lines, stellar spectra, spectra of explosive events such as novae and supernovae, the light from entire galaxies, x-ray lines of hot interstellar and intergalactic gas and gamma-ray lines of decaying unstable (but often long-lived) radioactive nuclei, and finally from the analysis of isotopic abundances in meteoritic inclusions.

The general concept of the synthesis of elements in the universe was formulated now more than 40 years ago by Burbidge *et al* [1]. The light elements (mainly hydrogen and helium) were made during the Big Bang, while the breeding places for most of the other elements are the interiors of stars or the burning fronts in stellar explosions. The stars generate energy by nuclear fusion processes, thus changing the initial abundances and forming new elements. These energy generation processes stabilize the star against gravitational contraction and allow it to shine for many millions of years depending on the nuclear timescale of the fusion processes. The nuclear reactions occur deep in the core of the star, but the freshly formed nuclei are eventually transported by sequences of convective dredge-up processes from the burning zones to the stellar atmosphere followed by mass loss due to radiation-pressure-driven winds. This scenario often forms planetary nebulae, observed as vast gas clouds surrounding a centre star. Alternative release mechanisms are stellar explosions, where the freshly produced nucleosynthesis products are expelled by an explosion shock front. In both cases the freshly bred nuclear material is mixed into the interstellar medium (ISM) and will become part of the initial abundance composition for new stars to be formed. Thus the galactic chemical evolution represents a 'cosmic cycle'; the ashes of stellar burning become the breeding material for new stellar generations. The observed elemental abundance distribution [2] reflects therefore the nucleosynthesis history of our universe; modelling and explaining these observed abundances requires simulations of the formation of a galaxy, its stellar mass distribution and the birth, evolution, lifetime and death of stars.

Stellar evolution is driven and controlled by a sequence of nuclear burning stages operating on nuclear fuel with increasingly higher charge numbers (hydrogen, helium, carbon, neon, oxygen, silicon) at increasingly higher core densities and temperatures. Parallel to these fusion processes in the stellar core, fuel with lower charge numbers is burnt in surrounding shells. Stars with masses $M < 10\ \mathrm{M}_{\odot}$ (with the solar mass $\mathrm{M}_{\odot}$) reach only in the centre conditions which are sufficient for core helium and carbon burning; these stars produce mainly carbon, nitrogen and half of the nuclei heavier than iron. More massive stars basically make the elements between oxygen and zinc, and, probably during their type II supernova explosion, also the other half of the elements heavier than iron. Finally, type Ia supernovae produce roughly half of the fraction of nuclei in the iron mass region, but also some portion of intermediate-mass nuclei.

While the elements lighter than $A \approx 60$ are made by charged-particle-induced fusion reactions, the heavier nuclides are produced by neutron capture reactions. These capture

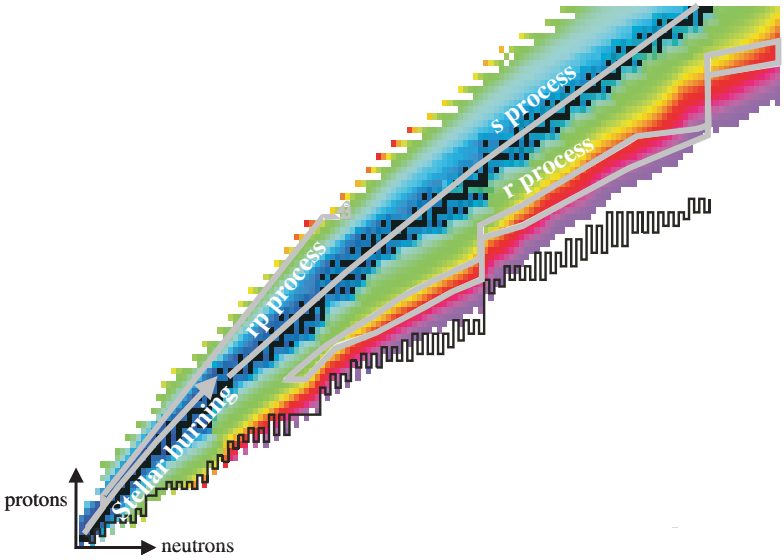

Figure 1. The chart of nuclei and the dominant pathways of astrophysical nucleosynthesis processes. The r-process occurs in dynamically changing astrophysical environments and thus covers a range of paths in the nuclear chart (courtesy of Hendrik Schatz).

reactions have to compete with nuclear β-decays. One distinguishes between the slow neutron capture process (short s-process), for which β-decay halflives τ_β are shorter than the competing neutron capture times τ_n, and the rapid neutron capture process (r-process), for which one has $\tau_n \ll \tau_\beta$. As τ_n is inversely proportional to the available neutron density, the r-process is expected to occur under extreme neutron fluxes and evolves through very neutron-rich, unstable nuclei. As $\tau_\beta < \tau_n$ for the s-process, the reaction path, in contrast, runs along the valley of stability. Figure 1 sketches the various astrophysical nucleosynthesis pathways within the nuclear chart.

Astrophysical timescales range from long-term stellar evolution processes ($\geqslant$1 Gyears) to rapid stellar explosion scenarios ($\leqslant$1 s). These timescales are determined by the microscopic timescales of the nuclear reaction and decay processes providing the associate energy generation and the observable luminosities of the event. These nuclear processes—sometimes in conjunction with convective processes—also characterize the rate of the associated nucleosynthesis mechanisms. It is therefore important to understand the microscopic nuclear physics basis of the macroscopic astrophysical events.

2. Big-Bang nucleosynthesis

Besides isotropy and homogeneity, the standard Big-Bang model assumes that the early universe is governed by the same laws of physics as today's universe. Based on the assumption that no other kinds of particle than known today existed during this period of nucleosynthesis, the thermal history of the early universe is reconstructable. One finds the relations [3]

$$T(t) \sim R(t)^{-1}; \qquad T(t) \approx \frac{1.3 \times 10^{10}}{t^{1/2}}\ \mathrm{K} \tag{1}$$

which describes the cooling of the universe (temperature T) as a function of the expansion (length scale R) and time (t in seconds). The evolution of the early universe is characterized by

a thermal equilibrium of the abundant particles existing at the temperature T. The equilibrium is ensured by reactions among these particles for which the rates are greater than the expansion rate of the universe. In thermal equilibrium, reactions proceed in both directions at the same rate; in particular this is valid for the particle-producing and particle-annihilating reactions

$$\text{particle} + \text{antiparticle} \leftrightarrow \text{photon}. \tag{2}$$

If the temperature decreases significantly below the mass of a particle ($kT < mc^2$), reaction (2) proceeds dominantly to the right; i.e. particles and antiparticles annihilate and die out. From equation (2) it seems that matter and antimatter should always exist in exactly the same amounts, but this is not necessarily the case (see e.g. [4]), as grand unification theories predict that the decay of the gauge bosons, which mediate the transformations of quarks and leptons at energies above 10^{18} MeV, violates the CP symmetry and thus might generate a small surplus of matter (nucleons, electrons) over antimatter (antinucleons, positrons). Consequently, at $T \approx 10^{12}$ K, all antinucleons would have annihilated with nucleons, leaving a tiny surplus of nucleons, which would then become the breeding material for the primordial (and later stellar) nucleosynthesis.

Besides a small concentration of protons and neutrons, at $T = 10^{12}$ K the universe initially was made mainly of electrons, positrons, neutrinos, antineutrinos and photons, which all existed in thermal and chemical equilibrium. The ratio of the number of protons, $N_{\mathrm{p}}(T)$, and neutrons, $N_{\mathrm{n}}(T)$, is determined by reactions mediated by the weak interaction:

$$\mathrm{n} + \nu \leftrightarrow \mathrm{p} + \mathrm{e}^-; \tag{3}$$

$$\mathrm{n} + \mathrm{e}^+ \leftrightarrow \mathrm{p} + \bar{\nu}; \tag{4}$$

$$\mathrm{n} \leftrightarrow \mathrm{p} + \mathrm{e}^- + \bar{\nu}. \tag{5}$$

Protons and neutrons also can fuse and form deuterons

$$\mathrm{n} + \mathrm{p} \leftrightarrow \gamma + \mathrm{d} \tag{6}$$

but the large number of energetic photons (the ratio of photons to baryons exceeds 10^9) immediately photo-dissociate the produced deuteron. Thus, a significant concentration of deuterons is not formed until the temperature drops considerably below the deuteron binding energy ($E_{\mathrm{B}} = 2.23$ MeV). Before this happens at $T \approx 10^9$ K (about 100 keV), two events occur which determine the $N_{\mathrm{n}}/N_{\mathrm{p}}$ ratio. First, the weak-interaction rates cannot keep pace with the expansion rates of the universe, and consequently neutrinos drop out of equilibrium. Secondly, electrons and positrons annihilate at $T \approx 5 \times 10^9$ K, heating up the photon bath, but not the neutrinos which are already decoupled. As a consequence of these two events, baryons and leptons decouple and the $N_{\mathrm{n}}(T)/N_{\mathrm{p}}(T)$ ratio is frozen at a constant value. Taking the neutron decay (5) into account one finds a ratio of one neutron to seven protons at the onset of nucleosynthesis at $T \approx 10^9$ K.

At $T \approx 10^9$ K, the primordial nucleosynthesis bottleneck is overcome when deuterons begin to form in significant concentration. The subsequent reactions proceed rapidly as (1) the binding energies of ^{3}H, ^{3}He and ^{4}He are larger than that of the deuteron and (2) the rates of the reactions d(p, γ)^{3}He, d(n, γ)^{3}H, d(d, p)^{3}H, d(d, n)^{3}He, ^{3}H(d, n)^{4}He, ^{3}He(d, p)^{4}He and ^{3}He(^{3}He, 2p)^{4}He are large. Primordial nucleosynthesis essentially comes to an end with the production of ^{4}He, as the nonexistence of stable nuclei with mass numbers 5 and 8, the growing Coulomb barrier between the nuclei and the rapidly falling temperature prevent the production of heavy nuclei. Primordial nucleosynthesis is finished at $T = 10^8$ K.

In the standard model, most of the existing neutrons are used essentially to produce ^{4}He, while only small traces of other light elements (deuteron, ^{3}He and ^{7}Li) are made. Simulations of primordial nucleosynthesis depend only on one free parameter, the baryon-to-photon ratio η.

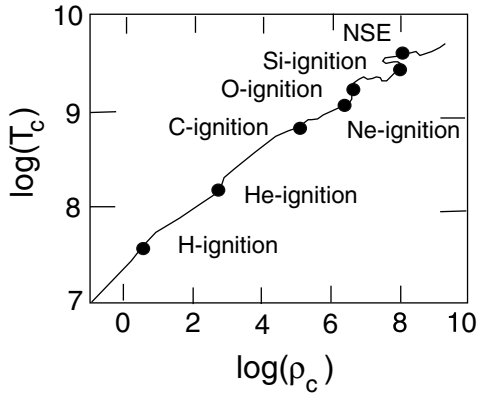

Figure 2. Development of temperature and density in the core of a 25 $M_\odot$ star during stellar evolution from the hydrogen burning phase to the onset of the supernova collapse phase. Indicated are the initiation conditions for the various burning stages prior to the nuclear statistical equilibrium phase (NSE) before collapse.

By comparing the calculated and observed primordial abundances for the elements d, ^{3}He, ^{4}He and ^{7}Li, the value for η can be restricted to [5]

$$2.9 \times 10^{-10} < \eta < 3.8 \times 10^{-10}. \tag{7}$$

From the value of η the mass density of baryons Ω_B in the universe can be deduced and one finds that Ω_B is only a few percent of the critical mass density Ω_{cr} necessary to just close our universe. From the fact that $\Omega_B/\Omega_{cr} < 1$, it is usually concluded that our universe must contain a dominant amount of dark matter if it is closed. This conjecture has been very recently confirmed in a spectacular way by two independent experiments. First, a survey of distant type Ia supernovae provides evidence for an accelerating expansion of the universe over the last several 10^9 years [6, 7]. Second, the balloon experiment BOOMERANG has measured the angular power spectrum of the cosmic microwave background [8]. Importantly, the observed spectrum contains multiple peaks and minima, as predicted by inflationary Big-Bang models. A combined analysis of the high-redshift supernovae results and the BOOMERANG data severely constrains the Big-Bang parameters [8]. A best fit is consistent with a flat ($\Omega = \Omega_{cr}$) universe. The baryon mass density is fitted as $\Omega_B h^2/\Omega_{cr} = 0.021 \pm 0.003$, in close agreement with the constraint derived from Big-Bang nucleosynthesis (h describes the current uncertainty in the value of the Hubble constant; $0.45 \leqslant h \leqslant 0.9$).

3. Stellar nucleosynthesis

The formation of elements heavier than $A = 4$ takes place inside stars at fairly high densities and temperatures. Such conditions are necessary to allow nuclei to interact and to overcome the Coulomb barrier. The different nucleosynthesis steps [9] are characterized by the subsequent phases of stellar evolution, which, depending on the initial mass of the star, lead to the formation of a white dwarf after significant radiation-driven mass loss or to the core collapse triggering a type II supernova event.

Static stellar burning is characterized by fairly 'low'-temperature conditions in the burning zone, $T \approx 2 \times 10^7$–5×10^7 K in massive main sequence stars, and $T \approx 5 \times 10^7$–3×10^8 K for red giant stars. Temperature and density in the stellar core gradually increase with time in dependence on the available nuclear fuel for providing stellar stability against gravitational contraction. Figure 2 indicates the development of core temperature and density during stellar evolution of a 25 $M_\odot$ star [10].

These temperatures correspond to a Gamow energy range from 20 to 120 keV for hydrogen burning and from 80 to 450 keV for helium burning, respectively. Typical reaction cross

sections at these energies are in the sub-nanobarn range and therefore extremely difficult to measure. For this reason most of the currently available reaction rates are based on the extrapolation of high-energy measurements down to the stellar energy range. This introduces significant uncertainties into the rates and the subsequent interpretation of stellar nucleosynthesis.

3.1. Stellar core burning

During hydrogen burning in the so-called main sequence stars four hydrogen atoms fuse to helium releasing about 25 MeV per fusion event. For stars with less than 1.5 solar mass the fusion process is dominated by the pp-chains. The slowest reaction, the p + p fusion to deuterium, determines the lifetime of the hydrogen burning phase. This reaction is mediated by weak interaction. Its present rate is based on theoretical calculations; the predictions for the reaction rate are generally believed to be quite accurate. However, there is no experimental confirmation for the reaction cross section of the p + p fusion process which determines the lifetime of our sun. Other critical reactions are the ^{3}He(α, γ)^{7}Be and ^{7}Be(p, γ)^{8}B capture processes, which determine to a certain extent the neutrino flux originating from low-mass stars. Detailed knowledge of the rates is necessary for the interpretation of the solar neutrino flux measured with solar neutrino detectors. For more massive stars the hydrogen burning is controlled by the CNO cycles, which have significant influence on the change of isotopic abundances of carbon and oxygen to nitrogen within the stellar core. The power generated by the CN cycle is limited by the slow ^{14}N(p, γ)^{15}O reaction, which also causes a nearly complete conversion of the initial carbon and oxygen content to ^{14}N. A recent evaluation of the solar fusion rates can be found in [11].

Red giant stars are identified as stars in their He-burning phase. The lifetime depends on the triple alpha reaction, the sequential fusion of three ^{4}He particles to ^{12}C. Since He-burning reactions are typically harder to measure than H-burning reactions (because of increased Coulomb barrier and higher background levels), some very basic questions concerning He burning still remain unanswered. The concept of the triple alpha reaction is understood; the rate is determined by the α-cluster structure of the associated compound nuclei ^{8}Be and ^{12}C and is extremely temperature sensitive. The ^{12}C(α, γ)^{16}O reaction is of enormous significance for late stellar evolution. It helps first to determine the mass of the core following He burning. Secondly, it determines—together with the ^{16}O(α, γ)^{20}Ne reaction—the C/O ratio, which in turn influences the following burning sequences of the star. The experimental determination of the reaction rate for ^{12}C(α, γ)^{16}O has been one of the major goals in nuclear astrophysics for the last three decades. However, the low cross section and the complexity of the low-energy reaction contributions handicap the prediction of a reliable rate severely [12–14].

Figure 3 shows the nucleosynthesis for light isotopes ($A \leqslant 22$) during the stellar hydrogen- and helium-burning phase for a 25 $M_{\odot}$ star. During the hydrogen-burning phase the initial solar CNO abundance distribution is more or less converted to ^{14}N; during subsequent helium burning ^{12}C and ^{16}O are freshly produced and ^{14}N is converted to ^{22}Ne. From all of the associated α-induced nuclear processes only ^{14}N(α, γ)^{18}O is known with sufficient accuracy [15]. All other α capture reaction rates carry large uncertainties due to our lack of knowledge about possible low-energy resonance contributions [16].

Helium burning is also responsible for producing neutrons that lead to the synthesis of heavy elements via the *s*-process. The actual neutron production processes are only marginally understood. This may have significant consequences for our present interpretation of *s*-process nucleosynthesis within the framework of stellar models (see below).

The subsequent heavy-ion-burning phases such as carbon and oxygen burning depend on the nucleosynthesis of ^{12}C and ^{16}O during the He-burning phase. The burning itself relies not

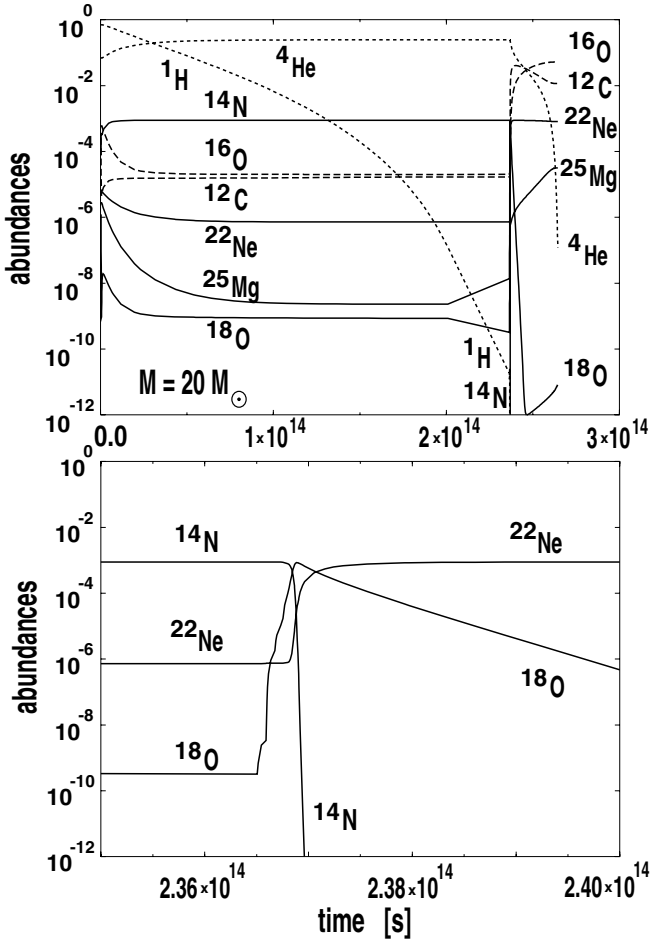

Figure 3. Nucleosynthesis of light isotopes during stellar hydrogen and helium burning of a 10 $M_\odot$ mass star. The upper panel shows the development of the isotopic abundances of ^{1}H and ^{4}He (dotted curves), ^{12}C and ^{16}O (dashed curves) and ^{14}N, ^{18}O, ^{22}Ne and ^{25}Mg. The lower panel shows the rapid depletion of ^{14}N into ^{18}O and subsequently into ^{22}Ne during the contraction phase of the core of the main sequence star and the ignition of helium burning.

only on the fusion processes, ^{12}C + ^{12}C, ^{12}C + ^{16}O and ^{16}O + ^{16}O, but also on many α and p capture processes on the fusion products. Burning stages beyond oxygen burning, which are relevant for the synthesis for nuclei heavier than calcium in the pre-supernova phase of the star, increasingly occur in a state of full or partial nuclear statistical equilibrium (NSE). Thus binding energies and partition functions of the nuclei involved mainly determine the abundances. As long as the 'freeze-out' is sufficiently rapid nucleosynthesis is less sensitive to individual reaction rates. Yet, reaction rates remain important for nucleosynthesis in the subsequent cooling phase of the event since the equilibrium breaks down below temperatures of roughly 3 billion K.

3.2. Stellar shell burning

Nucleosynthesis in the hydrogen- and helium-burning shells takes place at higher temperatures but lower densities than the corresponding core burning [9]. Therefore higher-Z nuclei

are involved in the process. Besides the CNO cycles reactions of the NeNa and the MgAl cycles can also take place in hydrogen-burning shells. In helium-burning shells of low- and intermediate-mass stars the main component of the s-process is triggered by the $^{13}C(\alpha, n)^{16}O$ reaction. Strong convective mixing processes characterize all these scenarios [17]. Material is rapidly mixed from cool zones into hot burning regions where rapid nucleosynthesis takes place; the freshly synthesized products are dredged up from the burning regions to the outer atmosphere of the stars and modify the surface composition substantially. These abundances are directly accessible to observation and offer one of the few opportunities to test directly our nucleosynthesis models [18]. This is possible by directly analysing the abundances of stellar atmospheres using spectrocopic means, which led in the early 1950s to the discovery of unstable technetium in stellar spectra, the first observational evidence for active nucleosynthesis [19]. The chemical analysis of meteoritic inclusions which have formed by condensation in the stellar winds of stars even permits us to determine isotopic abundance distribution directly, reflecting details of the nucleosynthesis history [20]. The comparison between the recent observational data and the model predictions indicates discrepancies. This is partly due to the treatment of convective processes in one-dimensional models but also partly due to the lack of reliable experimental reaction rates for proton and alpha-capture in the Ne/Si range.

3.3. The s-process

As discussed before the stellar helium-burning phases are the sites of the s-process. In this *slow* neutron capture process, heavy elements are built by a sequence of neutron captures and β-decays, mainly processing material from seed nuclei below and near the iron peak into a wide range of nuclei extending up to Pb and Bi. As the involved neutron capture times are usually significantly longer than the competing β-decays, the s-process path runs along the valley of stability in the nuclear chart. This allows the laboratory determination of the involved neutron-capture cross sections and half-lives, making the s-process probably the best understood nucleosynthesis network. It is observed that the product of neutron-capture cross sections and s-process abundances is locally a constant, supporting a steady-flow picture of the so-called classical model for the s-process [21, 22]. As neutron-capture cross sections are relatively small at magic neutron numbers, the s-process flow produces peaks related to the neutron numbers $N = 50, 82$ and 126.

The main uncertainties in s-process predictions are associated with the currently favoured stellar sites [23]. According to our current understanding, two s-process components are needed to reproduce the observed abundances. The $^{22}Ne(\alpha, n)^{25}Mg$ reaction, which occurs during helium core burning of CNO material, is believed to supply the neutrons for the weak component that produces the nuclides with $A < 90$ [24]. Helium flashes associated with rapid hydrogen mixing into the He-burning ^{12}C-enriched region are believed to be the site of the main s-process component that builds up the heavy elements up to the Pb and Bi range [25]. The infused hydrogen is captured on ^{12}C and provides the fuel for producing ^{13}C via $^{12}C(p, \gamma)\ ^{13}N(\beta, \nu)\ ^{13}C$. The subsequent $^{13}C(\alpha, n)\ ^{16}O$ reaction is considered the principal neutron source for the main s-process component. Both the nature and the extent of the convective processes as well as the low-energy reaction cross section for $^{13}C(\alpha, n)$ are largely unknown and are treated as free parameters in present stellar modelling approaches. Improved experimental information about the low-energy contributions in the neutron sources is necessary to develop improved modelling techniques which also treat the convection and mixing aspects in a self-consistent manner.

Experimental uncertainties are associated not only with the neutron sources but also with neutron capture processes. Impressive improvements have been achieved over the past ten

years in the measurement of the stellar neutron-capture cross sections for stable nuclei above Fe [26]. A great effort should also be devoted to the measurements of neutron cross sections of light and intermediate-mass nuclei. For these elements only old cross sections are in general available, with large uncertainties, but they may play a crucial role as neutron poison and will influence the composition of wind ejecta and dust grains [27]. Of particular importance is the close investigation of neutron capture reactions on long-lived β-unstable neutron-rich isotopes. These isotopes represent potential branching point nuclei in the reaction path. Detailed analysis of the observed s-process abundance distribution in conjunction with neutron capture measurement data on these branching point nuclei provide important information about the temperature, density and neutron flux conditions at the s-process site. Neutron capture measurements on branching point nuclei such as ^{79}Se, ^{85}Kr, ^{95}Zr, ^{107}Pd, ^{135,137}Cs, ^{141}Ce, ^{147}Pm, ^{151}Sm, ^{155}Eu, ^{169}Er, ^{170}Tm, ^{175}Yb, ^{186}Re, ^{204}Tl and ^{193}Pt therefore offer a unique tool for testing the stellar s-process models.

Traditionally it was believed that the s-process is the main source for the production of Pb isotopes, which represent the endpoint of the s-process. Recent observations of r-process abundance distribution in old metal-poor stars, however, imply that there may be a strong r-process component in Pb [28]. To fully simulate the endpoint of the s-process and the associated Pb production, measurements of neutron capture on Pb and Bi stable and long-lived isotopes are necessary.

3.4. Final burning phases of stellar evolution

After the exhaustion of the ^{4}He fuel in the stellar core, stars with $M > 8\ M_\odot$ during their late phases undergo further stages of evolution which are characterized by carbon, neon, oxygen and silicon burning, processes driven by heavy-ion fusion and by photodisintegration reactions. In the following, we concentrate on the discussion of the heavy-ion interactions in the carbon- and oxygen-burning phases.

Carbon-burning nucleosynthesis is characterized by the $^{12}C + {}^{12}C$ reaction and to a lesser extent by the $^{12}C + {}^{16}O$ fusion. The temperatures necessary for carbon burning range from 0.8 to 1.2 GK, which corresponds to a Gamow range between 1 and 3 MeV. The dominant reaction channels are ^{12}C(^{12}C, α) ^{20}Ne and ^{12}C(^{12}C, p) ^{23}Na producing ^{20}Ne and ^{23}Na as well as protons and alpha-particles. Parallel, rapid interactions between the reaction products change the overall abundance distribution further.

Photodisintegrations start to play a role in the final hot phase of the pre-supernova star when $30kT \approx Q$ (the Q-value of the inverse capture reaction). This ensures sufficient photon flux with energies $> Q$ and leads to Ne burning at $T > 1.5 \times 10^9$ K due to a small Q-value of $\approx$4 MeV. Neon burning is driven by the photodisintegration of the ^{20}Ne nuclei, which were formed during carbon burning, via the ^{20}Ne(γ, α) ^{16}O reaction. After most of the neon is photodisintegrated the subsequent oxygen-burning phase is triggered by ^{16}O(^{16}O, α) ^{28}Si, ^{16}O(^{16}O, p) ^{31}P and ^{16}O(^{16}O, n) ^{31}S. These reactions and the subsequent capture of the released alphas, protons and neutrons lead to the production of ^{28}Si and ^{32}S.

The final burning stage in stellar evolution is silicon burning at temperatures in excess of 3×10^9 K. Such temperatures permit photodisintegrations for the Q-values of 8–10 MeV along the valley of stability and also the penetration of the corresponding Coulomb barriers for charged particle captures. This ends in a thermodynamic equilibrium with an abundance distribution around Fe NSE. In such an NSE the abundance of each nucleus $Y_{(Z,A)}$ is only governed by chemical potentials and thus it is only dependent on temperature T, density ρ, its nuclear binding energy B and partition function $G(T)$, while fulfilling mass conservation $\sum_i A_i Y_i = 1$ and charge conservation $\sum_i Z_i Y_i = Y_e$ (the total number of protons is equal to

the net number of electrons). Y_e is changed by weak interactions (beta-decays and electron captures) on longer timescales, which are essential for a correct description of these late burning stages. While still approaching NSE, different nuclear mass regions, usually separated by closed shells and small Q-values, can already be in equlibrium with the background of free neutrons, protons and alphas, but such quasi-equilibrium (QSE) clusters have total abundances which are offset from their NSE values [29].

4. Nuclear input in core-collapse supernovae

Simulating core-collapse supernovae has been at the forefront of research in astrophysics for several decades and the general picture might very well be developed. Nevertheless, one-dimensional computer simulations currently fail to explode. Does this imply that some of the microphysics ingredients of the models are incorrect and need improvement or do supernova explosions rely on three-dimensional effects such as convection or rotation? Despite impressive progress, this fundamental question is still open. As we shall see below, much of the relevant microphysics relates to weak-interaction processes in nuclei or nuclear matter under extreme conditions (density and temperature). The description of such processes is rather evolved. However, progress in computer technology, the development of new or advanced many-body models and the new era of experimental facilities promise to remove the nuclear-physics-related uncertainties from the simulations. In this section we shall review recent progress and perspectives of nuclear-physics-related supernova physics, but first we shall summarize the currently favoured core-collapse supernova scenario.

4.1. Current supernova picture

At the end of hydrostatic burning, a massive star consists of concentric shells that are the remnants of its previous burning phases (hydrogen, helium, carbon, neon, oxygen, silicon). Iron is the final stage of nuclear fusion in hydrostatic burning, as the synthesis of any heavier element from lighter elements does not release energy; rather, energy must be used up. If the iron core exceeds the Chandrasekhar mass limit $M_{\rm Ch}$, electron degeneracy pressure cannot longer stabilize the core and it collapses. This collapse is very sensitive to the entropy and to the number of electrons per baryon, Y_e (note that $M_{\rm Ch} \sim Y_e^2$). In turn, these two quantities are mainly determined by weak-interaction processes, electron capture and beta-decay. First, in the final stage of stellar evolution, following oxygen shell burning, the Fermi energy of electrons is high enough that it becomes energetically favourable to capture electrons by nuclei. This shifts the distribution of nuclei present in the core to more neutron-rich material. As we shall see below, beta-decay for some of these nuclei becomes increasingly competative due to an increase in phase space related to larger Q_β-values. We also note that at the collapse temperatures involved reactions mediated by the strong and electromagnetic interactions are fast enough to proceed in equilibrium with their inverse. Thus the matter composition is given by nuclear statistical equilibrium, subject to the constraints of temperature, density and electron-to-baryon ratio.

Electron captures reduce the degeneracy pressure. Furthermore, as the neutrinos, produced in the weak processes, are radiated away, electron capture, β-decay and photodisintegration cost the core energy. As a consequence, the collapse is accelerated. An important change in the physics of the collapse occurs if the density reaches $\rho_{\rm trap} \approx 4 \times 10^{11}$ g cm^{-3}. Then neutrinos are essentially trapped in the core, as their diffusion time (due to coherent elastic scattering on nuclei) becomes larger than the collapse time. Shortly after neutrino trapping, at $\rho \approx 10^{12}$ g cm^{-3}, neutrinos are thermalized by inelastic scattering on electrons. Then all

reactions are (approximately) in equilibrium, including the weak processes discussed above. Neutrino cross sections are strongly dependent on their energy (low-energy neutrinos can sneak out from the core more easily than high-energy ones), which makes detailed neutrino transport modelling essential for the final collapse and explosion simulations.

The degeneracy of the (trapped) neutrino Fermi gas hinders a complete neutronization. As a consequence, Y_e remains rather large through the collapse [31], which, due to conservation of charge, implies that the number of protons must therefore also be large, and this can only be achieved in heavy nuclei. The collapse has a rather large order and the entropy remains small during the collapse [32].

After neutrino trapping, the collapse proceeds homologously [33], until nuclear densities (a few 10^{14} g cm^{-3}) are reached. As nuclear matter has a finite compressibility, the homologous core decelerates and bounces in response to the increased nuclear matter pressure; this eventually drives an outgoing shock wave into the outer core; i.e. the envelope of the iron core outside the homologous core. The core bounce with the formation of a shock wave is believed to be the mechanism that triggers a supernova explosion, but the energy available to the shock is not sufficient, and the shock will store its energy in the outer core, for example, by excitation of nuclei which are basically dissociated into free nucleons.

After the supernova has exploded, a compact remnant with a gravitational mass of the order of one solar mass is left behind; this mass is slightly increased to 1.3–1.5 solar masses in the first second after the bounce by accretion. The remnant is very lepton rich (electrons and neutrinos), the latter being trapped as their mean free paths in the dense matter is significantly shorter than the radius of the neutron star. It takes a fraction of a second [34] for the trapped neutrinos to diffuse out, giving most of their energy to the neutron star during that process and heating it up. The cooling of the proto-neutron star then proceeds by pair production of neutrinos of all three generations which diffuse out. After several tens of seconds the star becomes transparent to neutrinos and the neutrino luminosity drops significantly [35]. In the 'delayed supernova mechanism' [36], the shock wave can be revived by absorption of outward-diffusing neutrinos by nucleons. This process deposits energy in the layers between the nascent neutron star and the stalled prompt shock, increasing the pressure behind the shock, and the respective layers begin to expand, driving the shock outwards again, eventually leading to a supernova explosion.

The final evolution of massive stars is typically simulated in two steps. At first, the evolution through the various hydrodynamical burning phases is followed until the iron core contracts with velocities in excess of $\sim$1000 km s^{-1} everywhere. This defines—somewhat arbitrarily—the presupernova model, which is then the input for the actual collapse and explosion simulations. With respect to the input physics the two steps differ in important aspects. The presupernova evolution requires the consideration of a rather detailed nuclear network. However, the densities are still low enough for the neutrinos produced in the various weak-interaction processes to leave the star unhindered. During this phase neutrinos are just an energy sink, which cools the star rather efficiently. The role played by neutrinos changes dramatically during the collapse and is possibly essential for the understanding of the explosion mechanism. These phases depend critically on neutrino-induced processes and require detailed bookkeeping not only of the neutrino luminosities but also of their spectra and angular distributions. These requirements are computationally quite demanding and necessitate multi-group (i.e. neutrinos of different flavour and energy) Boltzmann neutrino transport [37, 38]. Advantageously the temperatures during the collapse and explosion are high enough that the matter composition is given by nuclear statistical equilibrium without the need of reaction networks for the strong and electromagnetic interactions.

4.2. Weak interactions in the presupernova evolution

In 1995 Woosley and Weaver calculated a standard set of presupernova models (WW models [39]) for a large range of stellar masses using the implicit hydrodynamics code Kepler (similar studies have been performed in [40]). This code is continuously improved if new physics becomes available. While most of the improvements lead to rather insignificant changes in the presupernova models, the recent revision of the stellar weak-interaction rates have rather important consequences, as we shall discuss in this subsection. We also note that the presupernova models depend crucially on the still insufficiently known $^{12}C(\alpha, \gamma)\,^{16}O$ reaction rate. Satisfyingly, the reaction S-factor used in the WW models (170 keV b) agrees rather well with the results deduced from the latest measurements.

The most important weak-interaction processes during the presupernova evolution are electron captures and beta-decays, which are both dominated by Fermi and Gamow–Teller (GT) transitions. While the treatment of Fermi transitions (only in beta-decays) is straightforward, the correct description of the GT transitions is a difficult problem in nuclear structure. In their pioneering work on the subject Fuller, Fowler and Newman (FFN) [41] estimated the rates assuming a single GT resonance, which they derived on the basis of the independent-particle model, supplemented by Fermi contributions and experimental data for low-lying transitions, whenever available. These authors also noted the importance of the 'backresonances' for beta-decay. These are excited states in the decaying nucleus which are connected by strong GT transitions to low-lying states in the daughter nucleus and, by thermal population and with increased phase space, can significantly contribute to the stellar beta-decay rates.

As shown by recent experimental data the GT distributions in nuclei are quenched compared with the independent-particle model (IPM) and are strongly fragmented over many states in the daughter nucleus. Both effects are caused by residual interaction among the valence nucleons and an accurate description of these correlations is essential for a reliable evaluation of the stellar weak-interaction rates due to the strong phase space energy dependence, particularly of the stellar electron capture rates. The shell model is the only known tool to reliably describe GT distributions in nuclei [42]. Its application to iron-mass nuclei in the middle of the pf shell as required in the presupernova collapse, however, has long been inhibited due to the extremely large model space dimensions involved. After significant progress in shell-model programming [43] and hardware development the situation has changed very recently and in [44] it has been demonstrated that state-of-the-art diagonalization studies, typically involving a few 10 million configurations, are indeed able to reproduce all relevant ingredients ($GT_{\pm}$ strength distributions for changing protons (neutrons) into neutrons (protons), level spectra and halflives) and hence have the predictive power to reliably calculate stellar weak-interaction rates. This program has recently been finished and stellar weak-interaction rates for nuclei with $A = 45$–65 have been calculated based on the shell-model results, supplemented by experimental data, wherever available. The shell-model rates were discussed and validated in [45]. It has been found that for pf-shell nuclei the shell-model electron-capture rates are smaller than the FFN rates by, on average, an order of magnitude, for the reasons explained in [45]. The situation is different for the beta-decay as the shell model and FFN rates are of the same magnitude for the most relevant nuclei.

To study the influence of the shell-model rates on presupernova models Heger *et al* [46,47] have repeated the calculations of Weaver and Woosley [39] keeping the stellar physics, except for the weak rates, as close to the original studies as possible. The new calculations have incorporated the shell-model weak-interaction rates for nuclei with mass numbers $A = 45$–65, supplemented by rates from Oda *et al* [48] for lighter nuclei. The earlier calculations of Weaver and Woosley used the FFN rates for electron capture and an older set of beta-decay rates [49].

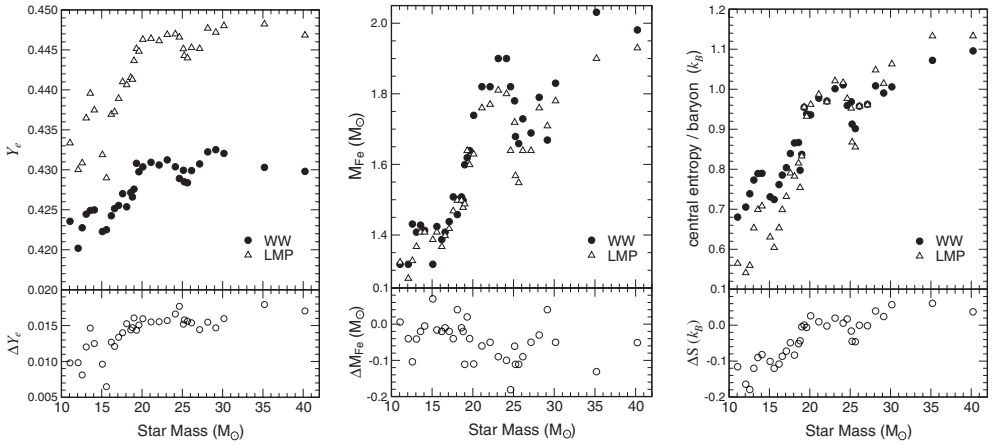

Figure 4. Comparison of the centre values of Y_e (left), the iron core sizes (middle) and the central entropy (right) for 11–40 $M_\odot$ stars between the WW models and those using the shell-model weak-interaction rates (LMP).

Figure 4 exemplifies the consequences of the shell-model weak-interaction rates for presupernova models in terms of the three decisive quantities: the central Y_e value and entropy and the iron core mass. The central values of Y_e at the onset of core collapse increase by 0.01–0.015 for the new rates. This is a significant effect. We note that the new models also result in lower core entropies for stars with $M \leqslant 20$ $M_\odot$, while for $M \geqslant 20$ $M_\odot$ the new models actually have a slightly larger entropy. The iron core masses are generally smaller in the new models where the effect is larger for more massive stars ($M \geqslant 20$ $M_\odot$), while for the most common supernovae ($M \leqslant 20$ $M_\odot$) the reduction is by about 0.05 $M_\odot$. (We define the iron core as the mass interior to the point where the composition becomes at least 50% of iron group elements ($A \geqslant 48$).) This reduction of the iron core mass appears to be counterintuitive at first glance with respect to the lower electron capture rates in the new models. It is, however, related to changes in the entropy profile during silicon shell burning, which reduces the growth of the iron core just prior to collapse [47].

To understand the origin of these differences it is illustrative to investigate the role of the weak-interaction rates in greater details. Weak processes become particularly important in reducing Y_e below 0.5 after oxygen depletion ($\sim 10^7$ and 10^6 s before core collapse for the 15 $M_\odot$ and 25 $M_\odot$ stars, respectively) and Y_e begins a decline which becomes precipitous during silicon burning. Initially electron capture occurs much more rapidly than beta-decay. As the shell-model rates are generally smaller than the FFN electron-capture rates, the initial reduction of Y_e is smaller in the new models; relatedly the temperature in these models is larger as less energy is radiated away by neutrino emission.

An important feature of the new models is that beta-decay becomes temporarily competitive with electron capture after silicon depletion in the core and during silicon shell burning (this was foreseen in [50]). The presence of an important beta-decay contribution has two effects. Obviously it counteracts the reduction of Y_e in the core, but, equally important, beta-decays are an additional neutrino source and thus they add to the cooling of the core and a reduction in entropy. This cooling can be quite efficient as often the average neutrino energy in the involved beta-decays is larger than for the competing electron captures. As a consequence the new models have significantly lower core temperatures than the WW models after silicon burning.

We note that the shell-model weak-interaction rates predict the presupernova evolution to proceed along a temperature–density–Y_e trajectory where the weak processes are dominated by nuclei rather close to stability. Thus it will be possible, after radioactive ion-beam facilities become operational, to further constrain the shell-model calculations by measuring relevant beta-decays and GT distributions for unstable nuclei. Reference [46] identifies the most important nuclei for both electron capture and beta-decay during the final stages of stellar evolution.

4.3. Weak-interaction rates during collapse

Obviously the differences in the central Y_e values will have effects on explosive nucleosynthesis, but, equally important, the relevant quantities (central Y_e and entropy and iron core size) are all changed by the new rates in a direction which apparently facilitates explosion. However, a preliminary evolution of the new 15 $M_\odot$ presupernova model during the collapse stage, including detailed neutrino Boltzmann transport, indicates that most of the differences present in the presupernova models are washed out during the collapse phase [51].

As stressed before, simulations of the collapse stage require detailed Boltzmann neutrino transport codes [52, 53]. Among the weak-interaction processes which have to be considered are neutrino absorption on free nucleons and on nuclei, elastic neutrino scattering off nucleons and nuclei, neutrino–electron scattering and neutrino–antineutrino pair production as well as the inverse processes; these include in particular the electron capture by nuclei and free protons. It turns out that the nuclear physics underlying these weak processes is generally approximated very crudely and calls for improvements. As an example, we mention that electron-capture rates on nuclei and the associated neutrino spectra, as adopted in these calculations so far [51, 54], are derived from an IPM consisting only of $f_{7/2}$, $f_{5/2}$ orbitals. Needless to say this model does not describe the relevant correlations for GT transitions adequately; it also predicts that the GT strength vanishes for neutron-rich nuclei with neutron number $N > 38$ as in these nuclei all final orbitals for GT transitions are blocked by neutrons. We shall briefly discuss recent approaches which promise more reliable estimates of the weak rates and neutrino spectra.

4.3.1. Electron capture on nuclei with neutron numbers $N > 40$. The simple nuclear models currently used to describe electron capture on finite nuclei during the collapse predict that GT transitions are totally blocked by the Pauli principle for nuclei with neutron numbers $N > 38$. Due to this artifact, it is observed in the collapse simulations that electron capture rates on nuclei drop drastically and cease once the core matter drives to neutron-rich material; the capture is then dominated by free protons. It has been pointed out [55] that this picture is too simple and that the blocking of the GT transitions will be overcome by thermal excitation, which either moves protons into $g_{9/2}$ orbitals or removes neutrons from the pf shell, in both ways reallowing GT transitions. In fact, Cooperstein and Wambach [55] found that, due to this 'thermal unblocking', GT transitions again dominate the electron capture on nuclei for temperatures of the order of 1.5 MeV. A similar unblocking effect is also expected by the residual interaction, which will mix the $g_{9/2}$ orbital with those in the pf shell, which is then already relevant at lower temperatures.

A consistent calculation of the electron capture rates for nuclei with neutron numbers $N > 40$ and proton numbers $N < 40$, including configuration mixing and finite temperature, is as yet unfeasible by direct shell-model diagonalization due to the large model spaces and many states involved. The task can, however, be reasonably well accomplished in a hybrid model suggested in [56]. The capture rates are calculated within an RPA approach with partial occupation formalism, including allowed and forbidden transitions. The partial occupation

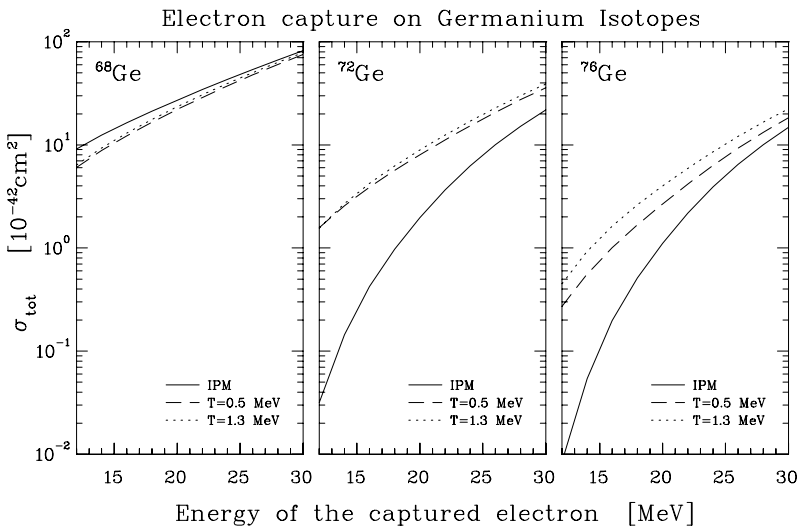

Figure 5. Electron-capture cross sections for ^{68}Ge (left), ^{72}Ge (middle) and ^{76}Ge (right) calculated within the IPM (solid) and for temperatures $T = 0.5$ and 1.3 MeV using the hybrid SMMC/RPA model as described in the text.

numbers represent an 'average' state of the parent nucleus and depend on temperature. They are calculated within the shell-model Monte Carlo (SMMC) approach at finite temperature [57] and including an appropriate residual interaction. In an explanatory study the electron capture on the even germanium isotopes $^{68-76}$Ge, corresponding to neutron numbers $N = 36$–44, has been calculated [56]. The SMMC calculations have been performed with a pairing + quadrupole force in the $pfg_{9/2}$ model space.

Figure 5 compares electron capture rates for ^{68,72,76}Ge calculated within the hybrid model for temperatures $T = 0.5$ and 1.3 MeV with the results in the IPM. As for ^{68}Ge the GT transitions are never totally blocked, they dominate the cross sections at stellar energies and the results in the IPM model and in the hybrid model do not differ too much. This is completely in contrast to ^{72,76}Ge, where the cross sections in the IPM are given by forbidden transitions (mainly induced by 1^- and 2^- multipoles). However, correlations and finite temperature unblock the GT transitions in the hybrid model, which increases the cross sections, in particular at low electron energies, significantly. Importantly we observed that the cross sections are rather similar for the two different temperatures, showing that the correlations, neglected in [55], are quite important in unblocking the GT transitions. The smaller cross sections for ^{76}Ge, compared with ^{72}Ge, simply reflect the larger Q-value for this nucleus.

4.3.2. Neutrino spectra from stellar electron capture. The neutrinos generated by electron capture on those nuclei present in the presupernova matter composition define the initial conditions for the detailed Boltzmann transport simulations. Recently these neutrino spectra have been calculated [58] based on the shell-model weak-interaction rates and the presupernova models discussed above [46]. Figure 6 shows the normalized spectra $n_\nu(E_\nu)$ for the six nuclei which dominate the weak flow in the presupernova model of a 15 $M_\odot$ star. All spectra show a rather similar, one-peak pattern, which can be well approximated by

$$n_\nu(E_\nu) = E_\nu^2(E_\nu - q)^2 \frac{N}{1 + \exp((E_\nu - q - \mu_e)/kT)} \tag{8}$$

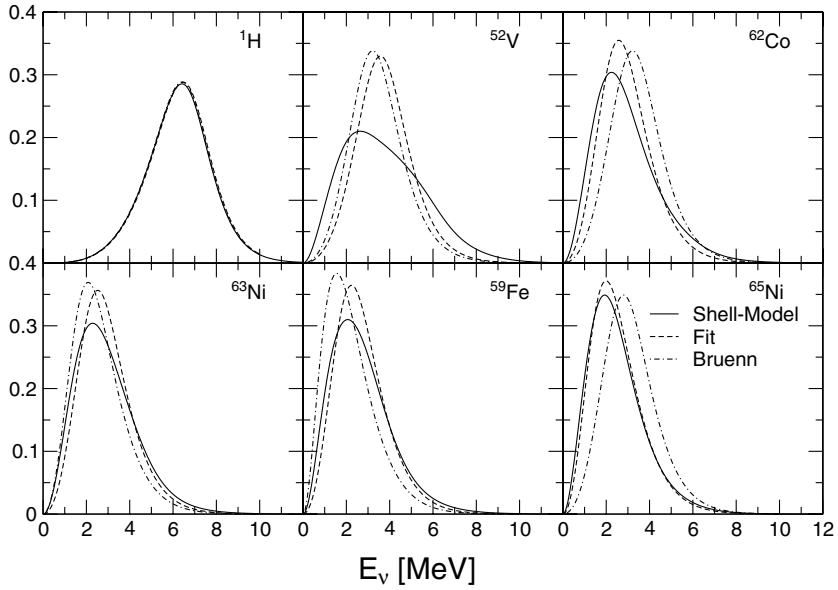

Figure 6. Normalized neutrino spectra from stellar electron capture. The calculations have been performed for the conditions of the presupernova model for a 15 $M_\odot$ star [46]. The plot shows the six most important electron-capturing nuclei. The solid curve shows the spectra derived from the shell-model description of electron capture [45], while the dashed curve is a fit using equation (22) to the shell-model spectra. The dashed–dotted curve gives the neutrino spectra proposed in [54].

where N is a normalization constant and the initial electron spectrum is given by a Fermi–Dirac distribution with temperature T and chemical potential μ_e. This rather simple form of the neutrino spectrum arises if (i) the electron capture on a state in the parent nucleus leads to a single state in the daughter nucleus at energy E_f and (ii) Brink's hypothesis is valid, i.e. this state is at $E_f + E_i$ if the capture is on an excited state in the parent at excitation energy E_i [58]. The parameter q is then given by $q = Q_0 - E_f$, where Q_0 is the reaction Q-value. This form is obviously valid for capture on free protons assuming the ultrarelativistic energy–momentum relation for the electron, which is a good approximation under collapse conditions.

At first glance it is surprising that such a simple spectrum follows for finite nuclei as the capture involves a thermal ensemble of several hundred states in the parent and daughter nuclei. To understand its origin we note that the electron chemical potential is high enough ($\mu_e = 8.1$ MeV in the present case) to allow efficient electron captures to the rather well concentrated collective GT states at a few MeV excitation energies in the daughter. Furthermore the shell-model calculations indicate that, in a good approximation, the giant GT resonances indeed obey the Brink hypothesis.

For finite nuclei, q should be considered a fit parameter. It can be adjusted to the average neutrino energy, which is listed in the shell-model rate tabulations for a grid of temperature/density points and can be easily interpolated in between. Examples of the obtained fit qualities are given in figure 6.

4.3.3. Neutrino-induced reactions. The most important neutrino reactions during collapse are coherent elastic scattering on nuclei and inelastic scattering of electrons. These reactions are mainly responsible for neutrino trapping and thermalization, respectively. However, it has

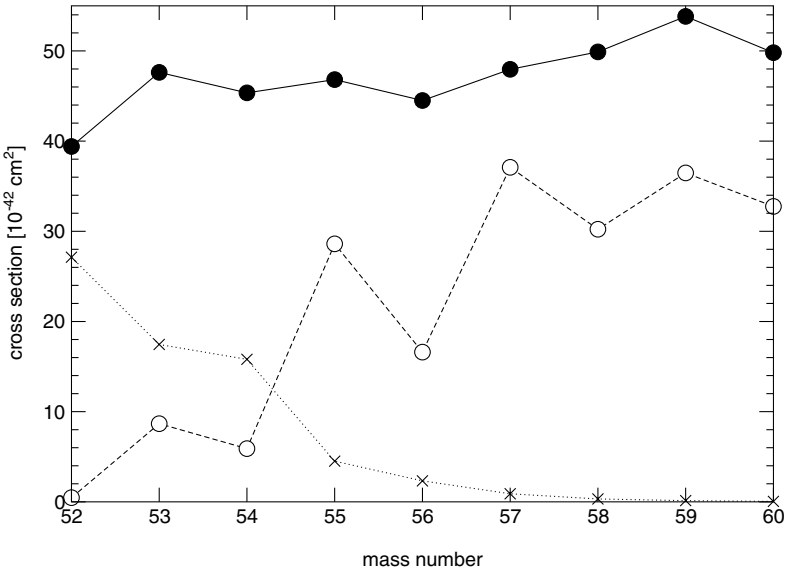

Figure 7. Neutral-current cross sections on iron isotopes calculated for a Fermi–Dirac neutrino energy distribution with temperature $T = 8$ MeV and zero chemical potential. The partial $(\nu, \nu' \mathrm{p})$ and $(\nu, \nu' \mathrm{n})$ cross sections are indicated by crosses and open circles, respectively.

been noted [59,60] that neutrino-induced reactions on nuclei can happen as well. To study this suggestion in detail, one has to know the charged- and neutral-current cross sections on nuclei as functions of neutrino energy. For pf-shell nuclei these quantities are again best derived within a hybrid model (GT transitions derived within the shell model and the other multipoles within an RPA approach). Within an isotope chain the (ν_e, e^-) cross sections increase with growing neutron excess $(N - Z)$ [61], which simply reflects the fact that Fermi and GT transitions, which dominate the cross sections, obey sumrules proportional to $(N - Z)$. The neutral-current cross sections are approximately the same for all nuclei (as is the total GT_0 strength); this has already been noted before for supernova neutrino distributions [62] (an example is shown in figure 7). The neutrino-induced reactions on the iron isotopes are discussed in detail in [61], which also gives $(\bar{\nu}, e^+)$ cross sections.

Finite-temperature effects on the neutrino–nucleus reaction rates have been studied by Sampaio *et al* [63, 64]. The effects are largest for small neutrino energies, where the cross sections at finite temperatures can be enlarged compared with that for $T = 0$, evaluated for the ground-state multipole responses, by several orders of magnitude. The origin of this increase is the giant resonances of the inverse processes (the backresonances) which are excited in the thermal ensemble. While the total rates for neutrino–nucleus reactions appear to be still smaller than the two most important neutrino reactions (elastic scattering off nuclei and inelastic scattering on electrons), it is important to note that in the backresonance contributions to the inelastic neutrino–nucleus scattering cross section the neutrino in the final state has picked up the nuclear excitation energy. Thus this process introduces a high-energy tail into the neutrino-energy distribution. For the charged-current processes the increase of the rates due to finite-temperature effects is unimportant for supernova processes as the electron chemical potential grows more rapidly than the temperature and the (ν_e, e^-) reaction is strongly Pauli blocked at low neutrino energies [63].

4.4. Delayed supernova mechanism

In the delayed supernova mechanism the fate of the explosion is determined by the competition of two distinct neutrino processes: neutrino pair production, by which matter loses energy, and neutrino absorption, which transfers energy to the matter. In a region inside a certain radius (the *gain radius*) pair production dominates, allowing the proto-neutron star to cool, while outside the gain radius matter is heated, which is primarily mediated by absorption of electron neutrinos and antineutrinos on free nucleons which have been previously deliberated by dissociation due to the shock. Due to the smaller abundances, neutrino-induced reactions on finite nuclei are expected to contribute only modestly to the shock revival. It has been also suggested that the shock revival is supported by 'preheating' [59]. In this scenario the electron neutrinos, which have been trapped in the homologous core during the final collapse phase, are deliberated in a very short burst (with luminosities of a few 10^{53} erg s^{-1} lasting for about 10 ms), which can partly dissociate the matter (e.g. iron and silicon isotopes) prior to the shock revival. As reliable neutrino-induced cross sections on nuclei have not been available until recently, the neutrino–nucleus reactions have not been included in collapse simulations.

The explosion depends crucially on the effectiveness by which energy is transported by neutrinos from the cooling proto-neutron star to the region where the shock has stalled. As stressed before, one-dimensional models fail to explode. However, this failure is 'marginal' and a rather small increase in the neutrino energy transport can transform the delayed supernova model into the long-searched-for robust explosion mechanism. It is conceivable that just this is achieved by two recently suggested improvements: (i) the effect of nucleon–nucleon correlations on the neutrino opacities in dense matter and (ii) the boost of neutrino transport by convection.

4.4.1. Neutrino opacities in dense matter. In his pioneering work, Sawyer [65] calculated the neutrino mean free path in uniform nuclear matter and showed that effects due to strong interaction are important. He also exploited the relation between the equation of state (EOS) of the matter and the long-wavelength excitations of the system to calculate the weak-interaction rates. However, consistency between the EOS and the neutrino opacities are more difficult to achieve for large energy (q_0) and momentum (q) transfer of the neutrinos. Here, particle–hole and particle–particle interactions are examples of effects which might influence the EOS and the neutrino opacities. For the following discussion it is quite illuminating to realize the similarity of the neutrino-induced excitations of nuclear matter with the physics of multipole giant resonances in finite nuclei.

For muon and tau neutrinos, neutral current reactions are the only source of opacities. Here, the energy and momentum transfer is limited by the matter temperature alone. For electron neutrinos the mean free path is dominated by charged-current ractions, for which the energy transfer is typically of the order of the difference between neutron and proton chemical potentials. During the early deleptonization epoch of the proto-neutron star the typical neutrino momenta are large ($\sim$100–200 MeV) and the mismatch of proton, neutron and electron Fermi momenta can be overcome by the neutrino momenta. This is no longer possible in later stages, when the neutrino energies are of the order of $k_B T$; then momentum conservation restricts the available phase space for the absorption reaction. For both charged-current and neutral-current reactions Pauli blocking of the lepton in the final state increase the mean free path.

We note an important and quite general consequence of the fact that muon and tau neutrinos react with the proto-neutron star matter only by neutral-current reactions. The four neutrino types have similar spectra (for neutrinos and antineutrinos the vector component in the interaction interferes constructively and destructively with the dominating axialvector

piece; the latter, however, dominates the cross sections); the spectra are usually assumed to be identical. Furthermore, these neutrino types decouple deepest in the star, i.e. at a higher temperature, than electron neutrinos and antineutrinos, and hence have higher energies. As the matter in the proto-neutron star is neutron rich, electron neutrinos, which are absorbed by neutrons, decouple at a larger radius than their antiparticles, which interact with protons by charged-current reactions. As a consequence decoupled electron neutrinos have, on average, smaller energies than electron antineutrinos.

For a much deeper and detailed description of the neutrino mean free paths in dense matter the reader is referred to [66] and the earlier work [67–69]. Here we shall only briefly summarize the essence of the work presented in these references.

Collapse simulations describe neutrino opacities typically on the mean-field level or even by a nucleon gas. Then an analytical expression can be derived for the vector and axialvector response of the medium, which in turn determines the charged- and neutral-current cross sections. Strong-interaction effects are considered by a medium-dependent effective mass in the dispersion relation. As in finite nuclei, collective excitations in nuclear matter arise due to nucleon–nucleon correlations beyond the mean-field approximation. As it is believed that single-pair excitations dominate over multi-pair excitations for the kinematics of interest to neutrino scattering and absorption, it appears to be sufficient to determine the vector and axialvector response, in a first step, within the random phase approximation (RPA). Assuming that the interaction is short ranged compared with the wavelength of the excitations, it is justified to retain only s-wave components in the interaction, which in turn can be related to Fermi-liquid parameters. It is found that the repulsive nature of the parameter G_0', which is related to the isovector spin-flip or giant GT resonances in nuclei, induces a collective state in the region $q_0/q \sim v_F$ (v_F is the Fermi velocity), while the cross section is reduced at smaller energies. However, these smaller energies are important for the neutrino mean free path at nuclear matter densities (ρ_0) or smaller densities. Assuming a typical neutrino energy $E_\nu = \pi T$ (corresponding to a Fermi–Dirac distribution with temperature T and zero chemical potential) RPA correlations increase the neutral-current neutrino mean free path (see figure 8) at low temperatures and for $\rho = \rho_0$, compared with the mean-field result. An enhancement due to RPA correlations is also found for neutrino absorption mean-free paths for neutrino-trapped matter. As in the case of neutrino-induced reactions on finite nuclei (see above), finite-temperature effects allow that nuclear excitation energy is transferred to the neutrino in inelastic scattering processes. This contributes to the cooling of the nuclear matter and increases the neutrino energy in the final state. Figure 9 shows an example for the expected energy transfer spectra, calculated in an RPA approach to nuclear matter at finite temperatures.

4.4.2. Convection. The observations from supernova 1987A imply large-scale mixing and overturn processes, which must reach deep into the exploding star ([71, 72] and references therein). These observations have triggered research into what role convection might play in the explosion mechanism, and it is found that convective processes might indeed be essential in the early explosion phase [71, 73].

One usually distinguishes two spatially separated regions of convection in a supernova: one region lies inside the neutrinosphere (referred to as proto-neutron star convection [51]), while the other one is located between the gain radius and the shock (neutrino-driven convection [51]).

Proto-neutron star convection is mainly driven by the negative lepton gradient which is established by the rapid loss of leptons in the region around the neutrinosphere [71]. By this mode hot, lepton-rich matter can be transported to the neutrinosphere. This increases the neutrino luminosities and hence helps the explosion. The simulation of proto-neutron star convection is additionally complicated by the fact that neutrinos and matter are strongly

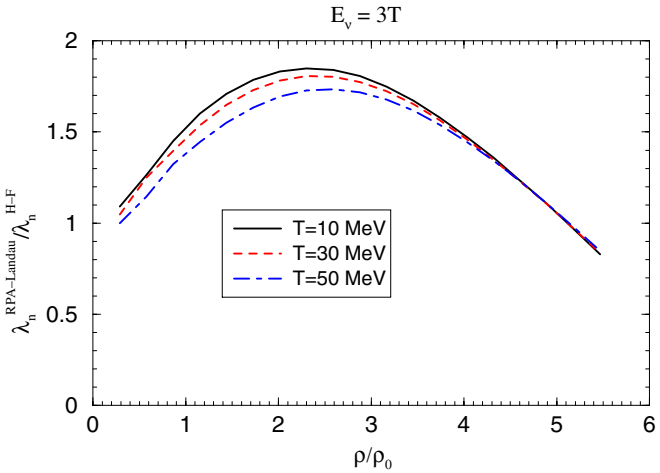

Figure 8. Ratio of neutrino mean free paths in neutron matter calculated in RPA and Hartree–Fock approaches at various temperatures [70]. The interaction is the Gogny force D1P. The neutrino energy is taken as $E_\nu = 3T$.

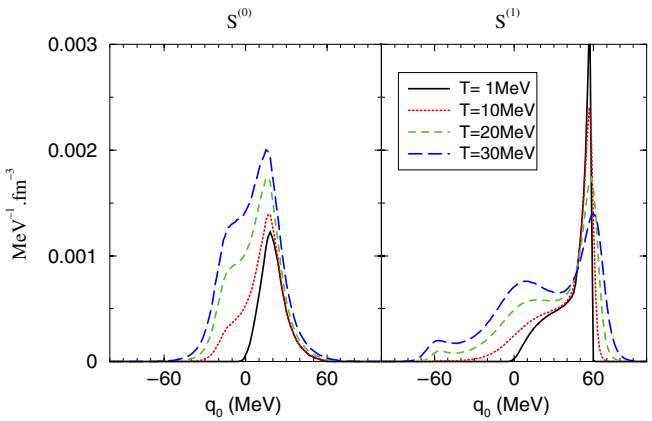

Figure 9. RPA structure functions (in the two spin channels $S = 0$ and 1) calculated in neutron matter with the Skyrme force SLy230a and at various temperatures [70]. The calculation has been performed for nuclear matter density ρ_0 and a momentum transfer of $q = 0.1k_F$.

coupled, thus requiring multi-dimensional hydrodynamics and neutrino transport simulations.

An attempt to simulate these effects has been reported by Wilson and Mayle [74], who introduced neutron-finger convection into their one-dimensional codes and then found supernova explosions. This model is based on the assumption that energy transport (by three neutrino flavours) is more efficient than lepton number transport (only by electron neutrinos). However, this assumption is currently under debate [75, 76].

Two-dimensional simulations of proto-neutron star convection have been reported by several authors (e.g. [53,71,77]). One interesting aspect of these simulations is the interplay of convection and neutrino transport. It is found that neutrino transport can equilibrate otherwise convective fluid elements [77]. Such a damping is possible in regions where neutrinos still strongly couple to the matter, but neutrino opacities are not too high to make neutrino transport

insufficient. In the model of Keil *et al* [53] the convective mixing occurs very deep inside the core where the neutrino opacities are high; no damping of the convection by neutrinos is found.

These calculations have clearly demonstrated that proto-neutron star convection exists and that, most likely, a rigorous three-dimensional treatment is needed.

Two-dimensional hydrodynamics simulations show large-scale overturns in the region between the gain radius and the stalled shock. Note that in this region the neutrinos have basically decoupled from matter, simplifying the treatment significantly. The convective motion shows rather narrow tubes of down-flowing cold (low-entropy) and dense matter and rising bubbles (plumes) of hot (high-entropy) material. Compared with one-dimensional treatments convection results in a more efficient transport of energy by neutrinos from the heated layers around and below the gain radius to the stalled shock, supporting its revival [72].

Early parameter-dependent studies found successful explosions [78, 79]. Describing the neutrino luminosities by an adjustable neutrino lightbulb approximation and exploring the parameter space Janka and Müller [71] concluded that neutrino-driven convection is only essential for successful explosions in a narrow parameter window [51]. Mezzacappa and collaborators [77] reported two-dimensional calculations in which neutrino-driven convection does not revive the shock.

4.5. Outlook

Despite some noteworthy progress in recent years, fundamental questions in supernova theory remain. For the evolution of the presupernova models, the largest uncertainty is probably still related to the astrophysically $^{12}C(\alpha, \gamma)^{16}O$ reaction rate (for recent progress, see [12–14]). Collapse models in one dimension, including Boltzmann neutrino transport, do not explode. If this remains unchanged by improvements of the input physics, such as realistic electron capture rates for nuclei with mass numbers $A \geqslant 65$ or neutrino-induced processes on nuclei, it might be a strong hint that multi-dimensional simulations including convection, magnetic fields and rotations are needed. These calculations are extremely challenging, but they appear to be necessary to explore the effects of convection in the proto-neutron star, where neutrinos and matter are strongly coupled, or to access the character of the neutrino-driven convection behind the shock. Another fundamental problem, which might hold the key to successful supernova simulations, is the realistic inclusion of nucleon correlations in the high-density neutrino opacities.

5. Nuclear physics of the r-process

About half of the elements heavier than mass number $A \sim 60$ are made within the r-process, a sequence of rapid neutron captures and β-decays [1, 80]. The process is thought to occur in environments with extremely high neutron densities. Then neutron captures are much faster than the competing decays and the r-process path runs through very neutron-rich, unstable nuclei. Once the neutron source ceases, the process stops and the produced nuclides decay towards stability, producing the neutron-rich heavier elements.

Many parameter studies of the reaction network, aimed at reproducing the observed r-process abundances, have progressed our general understanding, so it is generally accepted that the r-process operates in an environment with temperatures of the order of 10^9 K and with neutron densities in excess of 10^{20} cm^{-3}. Importantly it is found that the reaction network approximately proceeds in $(n, \gamma) \leftrightarrow (\gamma, n)$ equilibrium. Given the conditions for temperature and neutron densities this fixes the r-process to run along a path of constant neutron separation

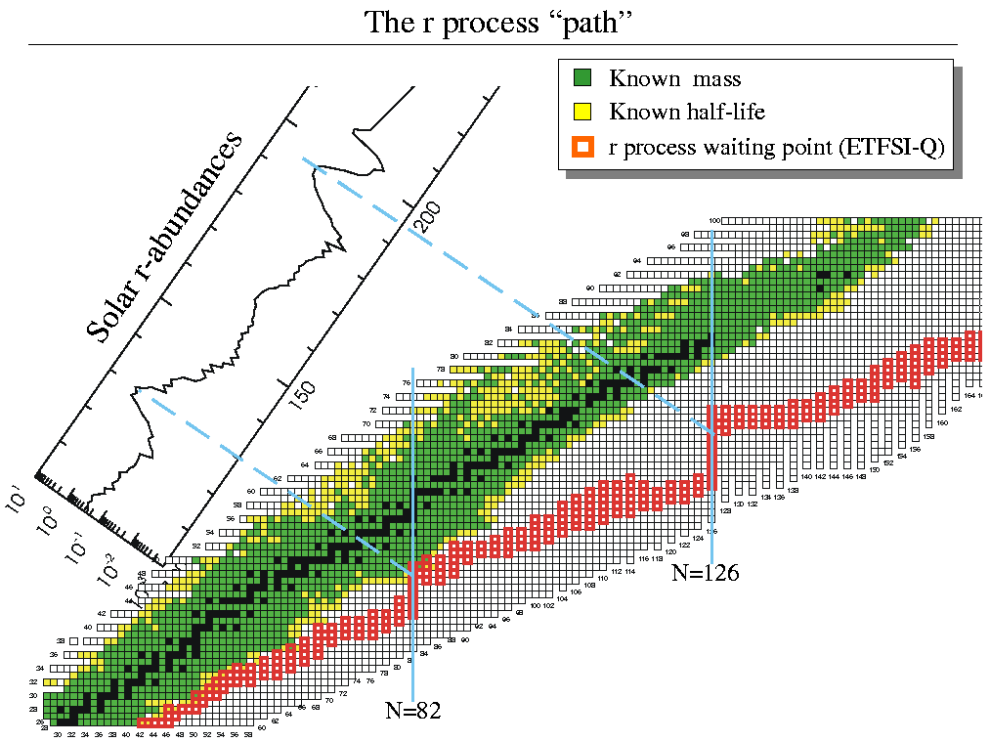

Figure 10. The r-process occurs under dynamically changing astrophysical conditions which affect the reaction pathway. The figure shows the range of r-process paths, defined by their waiting point nuclei. After decay to stability the abundances of the r-process progenitors produce the observed solar r-process abundance distribution. The r-process paths run generally through neutron-rich nuclei with experimentally unknown masses and halflives. In this calculation a mass formula based on the extended Thomas–Fermi model with Strutinski integral and special treatment of shell quenching (see the text) has been adopted (courtesy of Karl-Ludwig Kratz and Hendrik Schatz).

energies, $S_n \sim 2$–3 MeV [81] (see figure 10). This has two important consequences. At first, it immediately explains the observed peaks in the r-process abundances and relates them to the magic neutron numbers, $N = 50, 82, 126$: at the magic neutron numbers β-decays are relatively long and neutron separation energies are small, if compared with the non-magic nuclei along the r-process path. Thus the path runs through several, rather long β-decays at $N = 50, 82$ and 126 (the respective nuclei are called r-process waiting points) and a relatively large amount of matter is built up. Second, nuclei with such small neutron separation energies are so far away from stability that most of their required properties (i.e. mass, lifetime and neutron-capture cross sections) are experimentally unknown. Thus, these quantities have to be modelled, based on experimental guidance. As we shall discuss in the next section some progress has been achieved recently, but the real breakthrough is expected from future rare isotope facilities.

Despite many promising attempts the actual site of the r-process has not been undoubtedly identified. However, the parameter studies have given clear evidence that the observed r-process abundances cannot be reproduced at one site with constant temperature and neutron density. Thus the abundances require a superposition of several (at least three) r-process components [81]. This probably implies a dynamical r-process in an environment in which

the conditions change during the duration of the process. The currently favoured r-process sites (type II supernovae and neutron-star mergers) offer such dynamical scenarios. However, recent meteoritic clues might even point to more than one distinct site for our solar r-process abundance. The same conclusion can be derived from the observation of r-process abundances in low-metallicity stars, a milestone of r-process research. We shall summarize these exciting developments in the quest to determine the r-process site(s) in more detail below. Then we shall also briefly discuss that interesting constraints on the r-process site might also arise from an unlikely source, neutrino physics.

5.1. Nuclear r-process input

5.1.1. Nuclear masses. Arguably the most important nuclear ingredient in r-process simulations is the nuclear masses, as they determine the flow path. Unfortunately nearly all of them are experimentally unknown and have to be theoretically estimated. Traditionally this is done on the basis of parametrizations to the known masses. Although these empirical mass formulae achieve rather remarkable fits to the data (the standard deviation is of the order of 700 keV), extrapolation to unknown masses appears less certain and different mass formulae can predict quite different trends for the very neutron-rich nuclei of relevance to the r-process. The most commonly used parametrizations are based on the finite-range droplet model, developed by Möller and collaborators [82], and on the ETFSI (extended Thomas–Fermi with Strutinski integral) model of Pearson [83]. A new era has been opened very recently, as, for the first time, a nuclear mass table has been derived on the basis of a nuclear many-body theory (Hartree–Fock model plus BCS pairing) rather than by parameter fit to data [84].

Obviously, via their dependence on nuclear masses, r-process abundances are quite sensitive to nuclear structure effects. This dependence has been exploited twice in recent years to predict novel structure effects far from stability. A quite interesting discussion has arisen about the question whether shell gaps for r-process waiting points are significantly smaller ('quenched') than for stable magic nuclei. Such shell quenching has been predicted within Hartree–Fock–Bogoliubov calculations using a Skyrme force specially designed to account for continuum effects [85] and can correct the strong trough in the calculated r-process abundances at mass number $A \sim 115$ encountered with conventional mass formulae [86, 87]. On the experimental side, extensive measurements near the $Z = 50$, $N = 82$ double-closed-shell nucleus ^{132}Sn delivered astrophysically relevant information [88] and potentially also a first insight in the development of shell structure far from stability [89]. The chemically selective production of neutron-rich Ag isotope subsequently permitted detailed studies of the nuclear structure of Cd isotopes up to ^{132}Cd by β-delayed neutron and β-delayed γ-techniques [90]. While these data have been interpreted as evidence for shell quenching at the $N = 82$ shell closure, a direct experimental proof of this effect, albeit exciting, is still lacking. Very recent theoretical work discusses the subject rather controversially (e.g. [91]).

Another, however, somewhat milder trough in the calculated abundances compared with observation is found around $A \sim 160$. This discrepancy has been associated with nuclear deformation in the r-process nuclei in this mass range [92].

5.1.2. Halflives. The nuclear halflives determine the relative r-process abundances. In a simple β-flow equilibrium picture the elemental abundance is proportional to the halflife, with some corrections for β-delayed neutron emission [93]. As r-process halflives are longest for the magic nuclei, these waiting point nuclei determine the minimal r-process duration time, i.e. the time needed to build up the r-process peak around $A \sim 200$ via matter flow from the seed nucleus. We note, however, that this time depends also crucially on the r-process path.

Pioneering experiments to measure halflives of neutron-rich isotopes near the r-process path have been performed at the ISOLDE facility. The two $N = 50$ waiting point nuclei ^{80}Zn and ^{79}Cu and the first $N = 82$ waiting point nucleus ^{130}Cd have been identified within the last 15 years and their lifetimes have been measured [94]. Finally, the successful application of laser ion sources [95] led to the measurement of the halflife of the $N = 82$ waiting point nucleus ^{129}Ag. These data play crucial roles in constraining and testing nuclear models, which are still necessary to predict the bulk of halflives required in r-process simulations. It is generally assumed that the halflives are determined by allowed GT transitions. However, the β-decays only probe the weak low-energy tail of the GT distributions and provide quite a challenge to nuclear modelling as they are not constrained by sumrules. Traditionally the estimates of the halflives are based on either semiempirical global models or the quasiparticle RPA. Although these models generally do a reasonable job, a closer inspection against the few experimental r-process benchmarks reveals some insufficiencies. For example the FRDM halflives [82] show a significant odd–even staggering which is not present in the data, while the ETFSI halflives [83] appear globally too long. These shortcomings might have been overcome in recent calculations based on the HFB approach [96] or the interacting shell model [97, 98]. Both models obtain halflives in reasonable agreement with the available data. Importantly both models predict shorter halflives for the as yet unmeasured waiting point nuclei than the FRDM and ETFSI tabulations. We note, however, that no data for the $N = 126$ waiting point nuclei exist; hence models are here untested. Furthermore, while HFB calculations for the halflives of all r-process nuclei are conceivable and are actually being pursued, similar calculations within the shell model are still impossible due to computer memory limitations.

While the Q_β value for the decay of the neutron-rich r-process nuclei is large, the neutron separation energies are small. Hence β-decay can lead to final states above the neutron threshold and is hence accompanied by neutron emission. While the β-delayed neutron emission probabilities P_n are unimportant during the r-process (the $(n, \gamma) \leftrightarrow (\gamma, n)$ equilibrium guarantees recapture of the neutron), these quantities play a role at the end of the r-process when the neutron source has ceased and the produced nuclides decay to stability. The calculated P_n-values depend very sensitively on both the low-energy GT distribution and the neutron threshold energies. No model currently describes both quantities simultaneously with sufficient accuracy.

The halflives are generally derived assuming GT transitions. It has, however, been pointed out that forbidden transitions might contribute. This question clearly deserves further clarification. The odd-A nuclei such as ^{129}Ag are expected to exhibit a low-lying isomeric state, which might change the effective halflife of odd-A nuclei in the stellar environment. Shell-model calculations estimate the halflives of these isomeric states, however, rather close to the ground-state halflives [97].

5.1.3. Neutron-capture cross sections. For applications in r-process simulations neutron-capture cross sections are calculated within the statistical model. The validity of this approximation has been tested and justified in [99]. Crucial nuclear inputs into the statistical model calculations are level densities and dipole strength distributions [100]. Based on the pioneering work of Cameron and Gilbert, level densities are usually described within the backshifted Fermi gas model, although modern approaches consider experimentally known levels at low excitation energies explicitly.

Recently it has become possible to calculate nuclear level densities for pf-shell nuclei microscopically [101, 102], employing the SMMC technique developed by the Caltech group [57]. The SMMC describes the nucleus by a canonical ensemble at finite temperature and hence allows us to calculate the expectation value $E(T)$ as a function of temperature,

employing reasonable microscopic Hamiltonians. The energy spectrum $E(T)$ is related to the nuclear state density by an inverse Laplace transformation, which can be solved adopting a saddle-point approximation. The approach has been applied to many nuclei around $A \sim 60$ and it is found that the microscopic level density can be well approximated by a backshifted Fermi gas. As expected, the level density is strongly dependent on parity at low energies. A simple description to model this parity dependence is given in [103].

The γ-transitions in (n, γ) reactions are usually dominated by dipole transitions. It is further assumed that they can be represented by the tail of the giant dipole resonance (GDR). Based on a wealth of experimental data the GDR strength distribution in a nucleus can be well approximated by a Lorentzian shape with parameters compiled for example in [104].

It has been speculated that in nuclei with extreme neutron excess, i.e. for the r-process nuclei, collective dipole modes exist at energies noticeably lower than the GDR [105]. These modes, referred to as pygmy resonances, correspond to vibrations of the excess neutrons against the inert core composed of an equal number of protons and neutrons. If the pygmy resonances might reside at energies around the neutron threshold, they are expected to increase the (n, γ) cross sections. For example, recent relativistic mean-field calculations found evidence for a pygmy resonance in ^{208}Pb at $E^* = 7.3$ MeV, relatively close to the neutron threshold [106]. A parameter study of potential effects of pygmy resonances on the r-process abundances has been presented in [107].

5.2. Quest for the r-process site

There is growing evidence that more than one distinct r-process site has contributed to the observed r-process abundances. First evidence comes from recent observations of very old, metal-poor stars in the galactic halo, using the Hubble space telescope. These observations are arguably astronomical milestones as they determined the abundances of many r-process elements between $A \sim 110$ and 200 [108]. Strikingly, the observed r-process abundances in these stars have the same pattern as the solar distribution for $A > 130$, i.e. above the second r-process peak, while there are significant deviations from the solar pattern for $A < 130$, including an as yet unexplained odd–even staggering. These observations might imply that there is one site which produces the heavy r-process elements, while another site has to be added for the production of the lighter ones (however, see [109]). A similar conclusion is drawn by Wasserburg and collaborators [110, 111] on the basis of meteoritic data on the inventory of radioactive ^{129}I and ^{182}Hf in the early solar system. These authors suggest that two distinct type II supernova sources have been responsible for the observed r-process abundance. The first component, with an occurrence frequency of the order of 10^7 years, is responsible for the heavy r-process elements ($A > 130$), while a low-frequency component (10^8 years) makes the lighter elements.

What are possible r-process sites? As the r-process demands extremely high neutron densities and rather high temperatures, its site(s) is (are) probably associated with an explosive event. Within the last few years the neutrino-driven wind model has been widely discussed as a possible site of r-process nucleosynthesis [112, 113] and we shall discuss this model in more detail below. More recently the shock-processed helium shells in type II supernovae [114] as well as neutron mergers [115, 116] have been (re-) investigated as r-process sites.

5.2.1. The neutrino-driven wind model. Among these scenarios, the neutrino-driven wind model has attracted most attention in recent years. It is assumed that the r-process occurs in the layers heated by neutrino emission and evaporating from the hot proto-neutron star after core collapse in a type II supernova. In this model (e.g. [117]), a hot blob of matter with entropy per baryon S_b and electron-to-baryon ratio Y_e, initially consisting of neutrons, protons and

α-particles in nuclear statistical equilibrium, expands adiabatically and cools. Nucleons and nuclei combine to heavier nuclei, with some neutrons and α-particles remaining. Depending on the value of S_b, the nuclei produced are in the iron group or, at higher entropies, can have mass numbers $A = 80$–100. These nuclei then become the seeds and, together with the remaining neutrons, undergo an r-process. In this model a successful r-process depends mainly on four parameters: the entropy per baryon S_b, the dynamical timescale, the mass loss rate and the electron-to-baryon ratio Y_e. All parameters depend on the neutrino luminosity and are determined mostly by ν_e and $\bar{\nu}_e$ absorption on free nucleons. During a supernova explosion these parameters vary and the r-process in the hot neutrino bubble becomes a dynamical and time-dependent scenario, where the final abundances are obtained after integration over the duration of the r-process in the hot neutrino bubble (several seconds). Adopting the parameters of a supernova simulation by Wilson [36] Woosley and collaborators [112] obtained quite satisfying agreement between an r-process simulation and observation.

Despite these early successes, there has been criticism of the model and some open questions remain. There is now general concensus that the entropies used in the original work were probably too high. To understand the importance of the entropy, one has to consider that the production of seed nuclei has to go through the bottleneck of the three-body reaction $\alpha + \alpha + n \rightarrow {}^9\mathrm{Be}$ at the start. Due to the low Q-value of this reaction ($Q = 1.57$ MeV), a large entropy (or high photon number) drives this reaction in equilibrium to the left, ensuring a rather small amount of ^{9}Be. Since all ^{9}Be is basically transformed into seed nuclei, a high entropy results in a small number of seed nuclei and a large neutron-to-seed ratio n/s [120], which is required for a successful r-process. Systematic studies by Hofmann and collaborators [121] and Freiburghaus *et al* [117] have shown that a successful r-process requires either large entropies at the Y_e values currently obtained in supernova models, or smaller values for Y_e.

5.2.2. The role of neutrinos. Neutrinos are both a necessary requisite and a curse for the neutrino-driven wind model. The extreme flux of ν_e and $\bar{\nu}_e$ neutrinos from the proto-neutron star interact with the free protons and neutrons in the shocked matter by charge-current reactions. Via these reactions, neutrinos are the chief determinant of the proton-to-neutron ratio n/p or equivalently the Y_e value of the r-process matter. As shown by Fuller and Qian [122] one has the simple relation

$$\frac{\mathrm{n}}{\mathrm{p}} \approx \frac{L_{\bar{\nu}_e}\langle E_{\bar{\nu}_e}\rangle}{L_{\nu_e}\langle E_{\nu_e}\rangle}. \tag{9}$$

As the neutrino energy luminosities are about equal for all species ($L_\nu \sim 10^{52}$ erg s^{-1}), the n/p-ratio is set by the ratio of average energies for the antineutrino and neutrino. As discussed above, their different opacities in the proto-neutron star ensure that $\langle E_{\bar{\nu}_e}\rangle > \langle E_{\nu_e}\rangle$ and the matter is neutron rich, as required for a successful r-process.

While it is the neutrino absorption on nucleons which makes the r-process in this model possible, it is the subsequent neutrino interaction with α particles which might kill it again. We remember that the main freeze-out product from NSE in the high-entropy environment is *alpha*-particles. In a good approximation every available nucleon is incorporated into *alpha*-particles with some excess neutrons left (Fuller pointed out the isospin symmetry to Big-Bang nucleosynthesis [123]), which will become the source for the r-process. However, during the assembly of the α particles the free neutrons are still exposed to the large ν_e neutrino flux. As a consequence some of these neutrons are transformed into protons, which then, together with additional neutrons, are assembled into more *alpha*-particles. Thus, this α effect [124] severely reduces the final neutron-to-seed ratio and is therefore very counter-productive to a successful r-process.

A possible way out is to remove the matter very fast from the neutron star in order to reduce the neutrino fluxes for the α effect. Whether this can be dynamically achieved, for example by multi-dimensional effects, has to be investigated. Kajino and collaborators found that relativistic effects as well as nuclear reaction paths through neutron-rich light elements might also be helpful for a successful r-process [125]. Perhaps the most exciting solution to this dilemma could invoke new neutrino physics. Assume a mixing scheme of four neutrinos (three lighter active neutrinos and a heavier sterile type; such schemes have been suggested to solve the various neutrino problems). Then, as in the famous MSW effect, ν_e neutrinos might oscillate by matter enhancement into sterile neutrinos ν_s. These oscillations will decrease the rate of ν_e absorption on neutrons; hence n/p increases. This intriguing scenario is discussed in detail in [126].

There have been several suggestions for how neutrino-induced reactions on nuclei can play a role during and even after the r-process network. If the ejected matter flow reaches waiting point nuclei at rather small radii above the neutron star (say $\approx$ 100 km), ν_e-induced charged-current reactions can compete with the beta-decays of the longest-lived waiting point nuclei and thus speed up the matter flow to heavier nuclei [127]. It should be noticed, however, that neutrino capture on nuclei is not reduced at magic neutron numbers as the capture occurs from a reservoir of neutrinos whose energies are sufficiently high to allow for transitions to the IAS state or the GT resonant state [128]. Thus, at r-process freeze-out nuclear β-decay must dominate over neutrino capture to guarantee the production of the r-process abundance peaks. In turn, this requirement can be used as a constraint for the neutrino flux in the hot neutrino bubble, which is particularly useful if neutrino oscillations occur.

After the neutron supply ceases, the produced very neutron-rich progenitor nuclei undergo a series of beta-decays until they reach a stable nucleus, whose calculated abundance can then be compared with observation. During this period neutrino-induced reactions can spallate neutrons out of the target nuclei and hence influence the abundance distribution [127, 129].

Attempts to include neutrino-induced reactions in the r-process network within the neutrino-driven wind model have been reported in [130–132]. These authors considered charged-current cross sections which they estimated for allowed transitions on the basis of the IPM. Very recently a tabulation with charged- and neutral-current total and partial neutron spallation cross sections has become available for the neutron-rich r-process nuclei [133]. This tabulation is based on the RPA and considers allowed and forbidden transitions. Furthermore, the cross sections are tabulated for various supernova neutrino distributions, thus also allowing us to study the influence of complete neutrino oscillations on the r-process.

6. Neutrino nucleosynthesis

When the flux of neutrinos generated by the cooling of the neutron star passes through the overlying shells of heavy elements substantial nuclear transmutations are induced, despite the small neutrino–nucleus cross sections. Specific nuclei appear to be almost entirely (e.g. ^{11}B, ^{19}F) or in a large fraction (e.g. ^{10}B, ^{15}N) made by this neutrino nucleosynthesis [134, 135]. Within the ν-process these nuclei appear as the product of reaction sequences induced by neutral current (ν, ν') reactions on very abundant nuclei such as ^{12}C, ^{16}O or ^{20}Ne. If the inelastic excitation of these nuclei is to particle-unbound levels, these will decay by emission of protons or neutrons, in this way contributing to nucleosynthesis. As the nucleon thresholds in these nuclei are relatively high, effectively only ν_μ, ν_τ neutrinos (and their antiparticles) with their higher average energies ($\sim$25 MeV) contribute to the ν-process.

Neutrino-induced nucleon spallation on ^{12}C can make ^{11}B (which is partly made as the unstable ^{11}C), but this process can also knock out a deuteron or a proton–neutron pair, in

this way producing ^{10}B. The expected ^{10}B/^{11}B abundance ratio in neutrino nucleosynthesis is $\sim$0.05, which is significantly smaller than the observed abundance ratio, 0.25. Conventionally it has been assumed that the two nuclei are being made by reactions of energetic protons on ^{12}C in cosmic rays, which yields a ratio of ^{10}B/^{11}B of about 0.5, larger than the observed value. A solution might be that the two nuclides are being produced by both mechanisms, neutrino nucleosynthesis and cosmic ray spallation. It is interesting to note that the first process, being associated with supernovae, is a primary process, while the latter is a secondary process, as it requires the existence of protons and ^{12}C in the ISM. As a consequence the ^{10}B/^{11}B abundance ratio should have changed during the history of the galaxy. This can be tested once observers are able to distinguish between the abundances of the two different boron nuclides in stellar spectra [136].

Woosley *et al* [134] have also noticed that ^{180}Ta, the rarest element which only exists in a long-lived isomeric state, might also be produced by neutrino-induced neutron spallation of ^{181}Ta; an updated estimate based on more realistic neutrino cross sections is given in [137]. Conventionally it has been assumed that ^{180}Ta is made within the *s*-process. Under stellar conditions (finite temperature) it is decisive to know how strongly the long-lived isomeric state in ^{180}Ta (10^{15} years) couples to the short-lived ground state (8.15 h) to determine the effective halflife and thus the ^{180}Ta survival rate. The problem becomes complicated by convective modes during the *s*-process duration, which can transport the produced ^{180}Ta material to colder stellar zones, where it survives more easily. Based on a recent experiment [138] which measured the electromagnetic coupling of the ground and isomeric state via excited intermediate states and due to progress in stellar modelling of the convective modes in *s*-process scenarios, it appears conceivable that ^{180}Ta is also partly made within the *s*-process. The *p*-process has also been proposed [139] as another possible source for the production of ^{180}Ta.

7. Nucleocosmochronology

There are basically three different techniques to estimate the age of our universe. Two of them, based either on the observation of the expansion rate of the universe as implied by the velocities of distant galaxies or on the luminosities of the faintest white dwarfs, cannot give direct measurements of the age, as they rely on the assumptions about the observed objects [28]. The third approach is based on radioactive cosmochronology, exploiting the fact that some nuclides have lifetimes which are compatible with that of the universe. Two eon-glasses have been identified as particularly useful to estimate the age of the universe: ^{232}Th/^{238}U and ^{187}Re/^{187}Os.

The nuclei ^{232}Th and ^{238}U are *r*-process nuclei with halflives of 14 and 4.4 Gyears, respectively. If the *r*-process is indeed connected to core-collapse supernovae, some thorium and uranium together with other *r*-process elements should have been made at the fatal end following a relatively short life of high-mass stars made in the early history of our galaxy. The elements were then mixed into the ISM and some wound up in next-generation stars, where they should be observable. As mentioned above, *r*-process elemental abundances, including thorium, could indeed be determined in extremely metal-poor stars in the galactic halo recently [108]. The abundance ratio r of a radioactive (halflife $t_{1/2}$) and a stable comparison nuclide observed Δt Gyears after their production is then

$$r = r_0 \exp[-\ln 2 \Delta t / t_{1/2}], \tag{10}$$

where r_0 is the initial production ratio. This quantity has to be determined from *r*-process model and thus introduces a model dependence and a noticeable inaccuracy into age determinations. In a milestone event, the star CS32081-001 turned out to be so extremely low in iron abundance

that thorium and, for the first time, uranium could be detected in the same metal-poor star [140] (normally uranium lines are unobservable as they are superimposed by much stronger iron lines). While it is difficult to predict the production of either individually in supernovae, theoretical modelling of the ratio of the two nuclides which are only separated by two atomic numbers is noticeably less uncertain. Furthermore the different halflives of the nuclides makes the ratio a rather sensitive function of age. In fact applying equation (10) for both nuclides one finds

$$r_{\rm obs} = r_0 \exp[-21.8\Delta t]. \tag{11}$$

Cayrel *et al* have used their observed ^{238}U/^{232}Th abundance ratio from CS31082-001 and the r-process model predictions from [141, 142] to deduce $\Delta t = 12.5 \pm 3$ Gyears. If increased by about 0.1–0.3 Gyears to account for the time it took until the first high-mass supernovae occurred in the early history of the galaxy, a reasonable lower limit to the age of our universe is obtained.

While the uncertainty in the age determination for the U/Th pair arises from the nuclear physics input, this is different for the ^{187}Re/^{187}Os pair, as we shall discuss now. We start with the observation that the neighbouring nuclei ^{186}Os and ^{187}Os are both s-process-only nuclides, i.e. they are shielded against the r-process by the stable nuclei ^{186}W and ^{187}Re. Actually, ^{187}Re is not exactly stable, but has the long halflife of 42.3 Gyears, longer than the expected age of the universe. As noted by Clayton [143], this makes ^{187}Re/^{187}Os a clock for the age of the universe. The goal is achieved if the abundance of the parent (^{187}Re) is compared with that of the daughter (^{187}Os) when the s-only production of this daughter nucleus is subtracted from its total solar system abundance:

$$\frac{[^{187}{\rm Os}]_{\rm obs}}{[^{187}{\rm Re}\,]} = \frac{[^{187}{\rm Os}] - F_\sigma R_\sigma [^{186}{\rm Os}]}{[^{187}{\rm Re}\,]}. \tag{12}$$

An evaluation of this quantity requires the respective elemental abundances, which are known, and the ratio of neutron capture cross sections $R_\sigma = \sigma(186(n,\gamma))/\sigma(187(n,\gamma))$, averaged over a Maxwell–Boltzmann distribution of temperatures. Despite considerable efforts these cross sections are not known currently with sufficient accuracies. In particular neutron-capture data at very low neutron energies ($E_{\rm n} < 3$ keV) are needed. A further complication arises from the fact that ^{187}Os has a low-lying excited state at only $E_x = 9.8$ keV, which is virtually totally populated at the temperatures $T \sim 8$–30 keV at which s-process nucleosynthesis occurs in stars. The respective neutron-capture cross section on the excited state cannot be measured directly in the laboratory, but it can be indirectly determined from inelastic excitation of this state in (n, n') experiments [144]. The factor F_σ in the expression above accounts for the corrections of the cross section ratio due to finite-temperature effects.

Noticeable improvement of the neutron-capture cross section data on the osmium isotopes, including ^{186}Os and ^{187}Os, is expected from the n-TOF facility at CERN, which started to be available for nuclear astrophysics experiments in spring 2001. Once these data are available, the nuclear physics uncertainties in the Os/Re clock are under control. However, if one wishes to translate this knowledge into an age of the universe it is also necessary to know the chemical evolution of these nuclides over the age of our galaxy. This situation is less certain. It involves s-process modeling and astration of the nuclides in stars as well as assumptions about the time distribution of supernovae in the galaxy.

We note that the halflife of ^{187}Re is also strongly temperature dependent. However, experimenters at the GSI storage ring succeeded in measuring the halflife of bare ^{187}Re, which is 32.9 ± 2.0 years and thus nine orders of magnitude shorter than that of atomic ^{187}Re. The GSI data can be translated into a log ft value from which the halflife of ^{187}Re can be calculated in any ionization state [145].

8. Nucleosynthesis in explosive binary systems

Over the last 20 years thermonuclear explosions in accreting binary star systems have been an object of considerable attention. The basic concept of the explosion mechanism seems reasonably well understood but there are still considerable discrepancies between the predicted observables and the actual observations. The proposed mechanism involves binary systems with one (or two) degenerate objects, such as white dwarfs or neutron stars, and is characterized by the revival of the dormant objects via mass overflow and accretion from the binary companion. This leads to explosive events such as novae, type Ia supernovae, x-ray bursts and x-ray pulsars. The characteristic differences in the luminosity, timescale and periodicity depend on the accretion rate and on the nature of the accreting object. Low accretion rates lead to a pile-up of unburned hydrogen, causing the ignition of hydrogen burning via pp-chains and CNO cycles with pycnonuclear enhancements of the reactions after a critical mass layer is attained. On white dwarfs this triggers nova events; on neutron stars it results in x-ray bursts. High accretion rates above a critical limit on the other hand cause high temperatures in the accreted envelope and less degenerate conditions, which result in stable H burning or only weak flashes. High accretion rates on white dwarfs may cause supernovae type Ia events; accretion rates high enough for stable burning on a neutron star occur in highly magnetic x-ray pulsars. The present modelling of the accretion and thermonuclear runaway process is still in its infancy mainly due to the complex aspects of the explosion mechanism, which requires three-dimensional modelling techniques for realistic treatment [146]. Besides the complexities of asymmetric ignition and burning front development and the issues of rapid convection and mixing during the explosion large uncertainties are also associated with the microscopic nuclear physics component of the process. The nuclear energy generation provides the observed luminosity of the event; the combination of rapid mixing, convection and far-off-stability nucleosynthesis is responsible for the observed abundance distribution in the ejecta. These events are the largest thermonuclear explosions in the universe, synthesize a number of important isotopes that make up our world and serve as laboratories for nuclear physics at extreme temperatures and densities.

8.1. Nova explosions

Novae have been interpreted as thermonuclear runaways on the surface in close binary star systems [147]. Accretion processes or mass exchange between the two binary stars can take place when at least one of the stars fills its Roche lobe, which is the gravitational equipotential surface enclosing both stars. The matter of the extended star accretes through the Roche lobe onto the surface of the second companion, which represents a deeper gravitational potential. Novae are identified as binary systems with an extended near main sequence star filling its Roche lobe accreting matter onto the surface of a white dwarf companion. The accreted material forms a thin, but high-density, electron degenerate envelope at the surface of the white dwarf. Dredge-up of white dwarf material (^{4}He, ^{12}C, ^{16}O in the case of a CO white dwarf, ^{16}O, ^{20}Ne and ^{24}Mg in the case of an ONeMg white dwarf) into the envelope leads to an enrichment of the accreted material in heavier isotopes [148].

After a 'critical' mass has been accreted, thermonuclear ignition takes place at the bottom of the accreted envelope. This depends critically on the mass of the white dwarf and the accretion rate, which determines the pressure conditions at the bottom of the envelope. The ignition occurs presumably via the pp-chains; this causes at degenerate conditions a rapid increase in temperature at constant pressure and density. This 'thermonuclear runaway' is further enhanced by the subsequent ignition of the hot CNO cycles on the high abundances of

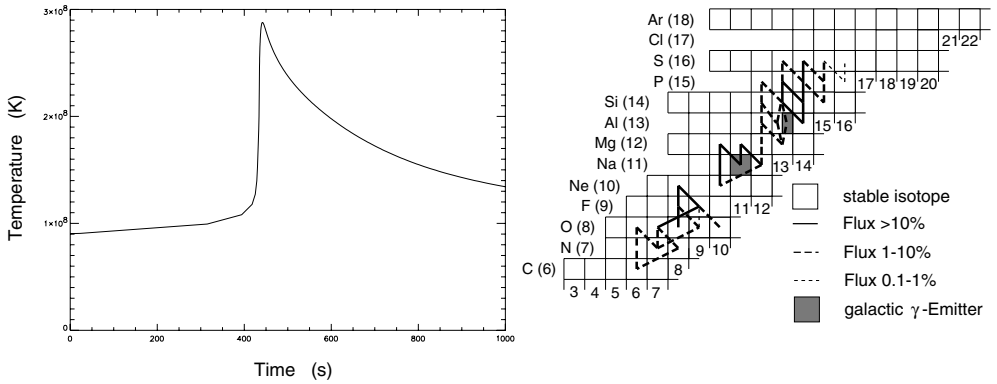

Figure 11. The left-hand panel shows the temperature curve during the thermonuclear runaway of a nova. The right-hand panel indicates the nuclear burning path associated with the thermonuclear runaway. While the main bulk of the energy generation is provided by the hot CNO cycles, interesting nucleosynthesis aspects are expected from the NeNa and the MgAl cycles, which are triggered by proton capture processes on Ne and Mg material mixed in from an O–Ne–M white dwarf.

^{12}C and ^{16}O until the degeneracy is lifted after the Fermi temperature $T_{\rm F}$ has been reached. The Fermi temperature depends on the density ρ (in g cm^{-3}) and the composition of the accreted material with $\mu_{\rm e}$ as electron mean molecular weight,

$$T_{\rm F} = 3.03 \times 10^5 \left(\frac{\rho}{\mu_{\rm e}}\right)^{2/3}, \tag{13}$$

i.e. the higher the density of the material the higher the peak temperature which can be reached in the thermal runaway before degeneracy is lifted. However, if the shell temperature is rising rapidly the peak temperature can exceed the Fermi temperature before the electron gas is sufficiently degenerate to initiate expansion. Due to the rapid temperature increase at the bottom of the envelope a convective zone develops which gradually grows to the surface as the temperature continues to increase. This allows rapid energy transport to the surface within the convective timescale of $t_{\rm conv} \approx 10^2$ s. Within that short timescale an appreciable fraction of the long-lived β^+ emitters which are produced by the hot CNO cycles is also carried to the surface. The release of decay energy further increases the luminosity to values above 10^5 L$_\odot$. The large amount of energy deposited in the outer layers on the short convective timescale, coupled with high luminosity often exceeding the Eddington limit $L_{\rm edd}$ [149], causes rapid expansion of the outer layers and the ejection of the outer shells.

Typical novae are characterized by thermal runaways with densities of approximately $\rho \approx 10^3$ g cm^{-3} and typical peak temperatures between 1×10^8 and 4×10^8 K [150]. Figure 11 shows for demonstration a temperature profile of the thermonuclear runaway of a classical nova model calculated for the hydrogen-burning zone at the bottom of the envelope of an accreting 1.0 M$_\odot$ white dwarf [150].

The main observables for a reliable interpretation of the explosion mechanisms are the nova light curve and the abundance distribution in the ejected material. The luminosity yields information on the total energy release from nuclear reaction and decay processes but it also gives information about the timescale of the thermonuclear runaway. The abundance observation gives evidence for the on-site nucleosynthesis but may also provide a tool for monitoring the rather complex mixing and convective mechanisms prior to and during the explosion. For a reliable interpretation of such observations improved nuclear physics input

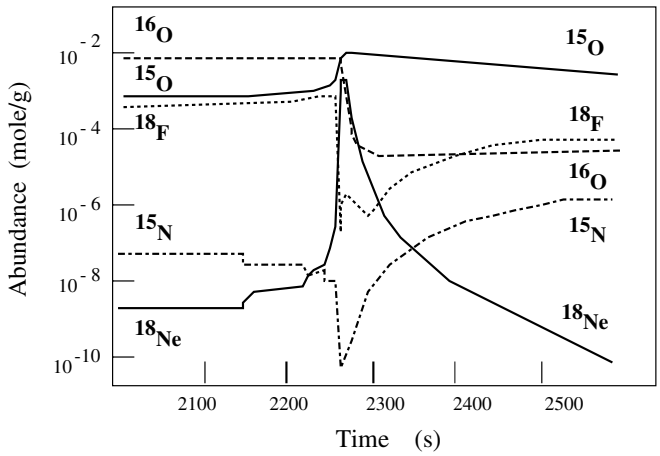

Figure 12. Nucleosynthesis of CNO isotopes during a nova explosion.

in the present nova models is crucial. The actual ignition temperature for novae is well below these peak temperatures. Rates of many nuclear reactions are therefore needed at energies below a few hundred keV to obtain a complete description of the ignition process in the various accreted layers of material. The main energy generation in a nova comes from the hot (or β-limited) CNO cycles ^{12}C(p, γ) ^{13}N(p, γ) ^{14}O(β, ν) ^{14}N(p, α) ^{15}O(β, ν) ^{15}N(p, α) ^{12}C and is determined by the rather long lifetimes of the ^{14}O and ^{15}O oxygen isotopes. This causes enrichment in ^{14}O and ^{15}O, which is observed as nitrogen enrichment in the ejecta. The actual energy generation rate is limited by the β-decay rates but is also affected by the hydrogen and CNO fuel available. A more quantitative interpretation of the actual nucleosynthesis therefore requires detailed knowledge of the associated convective processes, which may transport freshly produced material out of the actual hot burning zone or may bring more hydrogen fuel into the burning zone. In addition, the fuel balance may also change due to additional proton capture processes on short-lived radioactive nuclei in the CNO range [151]. Of particular relevance are the timescales for reaction sequences such as ^{16}O(p, γ) ^{17}F(p, γ) ^{18}Ne(β, ν) ^{18}F(p, α) ^{15}O, which would control fast additional fuel supply for the hot CNO cycle. Figure 12 shows the abundance development of CNO isotopes during the nova explosion.

Observations of over-abundances in the Ne to S mass range characterize Ne novae, which are interpreted to be thermonuclear runaways on accreting O–Ne white dwarfs with infusion of oxygen and neon (and magnesium) into the accreting envelope [152]. The nature of this mixing process is not understood. Proton capture reactions on the initial ^{20}Ne and ^{24}Mg lead to the production of heavier isotopes up to ^{32}S. This agrees well with recent observations in nova ejecta of silicon and sulphur [153]. According to theoretical model simulations considerable production of the long-lived radioisotopes ^{22}Na and ^{26}Al is expected [150, 154] in Ne novae. However, recent observations of the gamma activity in novae with the COMPTEL observatory gave no indication of ^{22}Na or ^{26}Al activity. There is an order of magnitude discrepancy between predicted and observed intensities of the ^{22}Na gamma-ray [155]. Studies of the nuclear reactions crucial to the synthesis of these radioisotopes are therefore particularly important. Recently a series of self-consistent calculations for nova nucleosynthesis have been performed for different sets of nuclear reaction rates [153, 156]. The results clearly indicate significant impact of nuclear reaction rates on fast nova nucleosynthesis.

Current nova models predict significantly less mass of ejected material than is observed.

Solutions to this problem suggest that peak temperatures in nova explosions may be much higher than (the currently accepted) 400 million K. Such high temperatures imply that break-out of the hot CNO cycle can occur for some novae—agreeing with at least one recent nova observation. The nuclear physics information required to understand this higher-temperature burning includes measurements of nuclear reactions on proton-rich unstable isotopes. Furthermore, reactions on isotopes above mass 40—the traditional endpoint of nova nucleosynthesis studies—need to be pursued to understand this higher-temperature nuclear burning.

8.2. Type Ia supernovae

Type Ia supernovae are characterized by the lack of hydrogen lines in their spectra, presumably because there is no extended hydrogen envelope. While several interpretations of the actual explosion mechanism exist, observational evidence points towards thermonuclear explosions of accreting white dwarfs with high accretion rates. The accreted hydrogen is rapidly converted to helium and subsequently via stable He burning to carbon and oxygen, which sediments on the surface of the C/O white dwarf. If the growing mass of the white dwarf exceeds the Chandrasekhar mass, contraction sets in and the carbon in the centre ignites by fusion reactions with screening enhancements. Whether this ignition happens at a singular point or at several different places in the centre is an open question. Note that in a highly degenerate object such as a white dwarf the energy release of the nuclear burning is used to increase the temperature rather than causing expansion as during hydrostatic stellar burning. This in turn drastically increases the nuclear reaction rates, triggering a thermonuclear runaway. This causes expansion and convective instabilities, leading to burning front propagation, which accelerates presumably to supersonic speed and finally turns into a detonation, causing complete disruption without a remnant. The propagation of the burning front occurs initially via heat conduction in the degenerate electron gas (requiring a spatial resolution in hydrodynamic calculations of the order 10^{-4}–10^{-5} cm), which is one of the major challenges in simulations of type Ia supernovae. It appears well established that electron capture will occur in the burning front, driving the matter to larger neutron excess, and thus strongly influences the composition of the ejected matter and the dynamics of the explosion. Type Ia supernova explosions are typically associated with a large amount of ^{56}Ni formation [157] and hence are considered the main producers of Fe-peak elements in the galaxy. Electron captures on the incinerated material, plus the neutron excess previously stored in the He-burning product ^{22}Ne, lead to the production of isotopes such as ^{54}Fe, ^{58}Ni and other neutron-rich nuclei such as ^{48}Ca, ^{50}Ti and ^{54}Cr. The final amounts depend critically on the propagation speed of the burning front.

While the type Ia supernova mechanism seems in general to be understood, many issues are still under debate [157]. This includes the masses of the stars in the binary system, the mass accretion history and composition, the matter transport during the explosion and the velocity of the burning front. These quantities have to be modelled and the resulting output (elemental abundances and their velocity distributions) is compared with observation, allowing us to check the models. However, the results are also strongly affected by the weak-interaction rates and the shell-model rates promise to remove this additional uncertainty from the models. Preliminary studies look very promising as the new rates apparently remove the overproduction of very neutron-rich isotopes, encountered in previous calculations with the FFN rates [158].

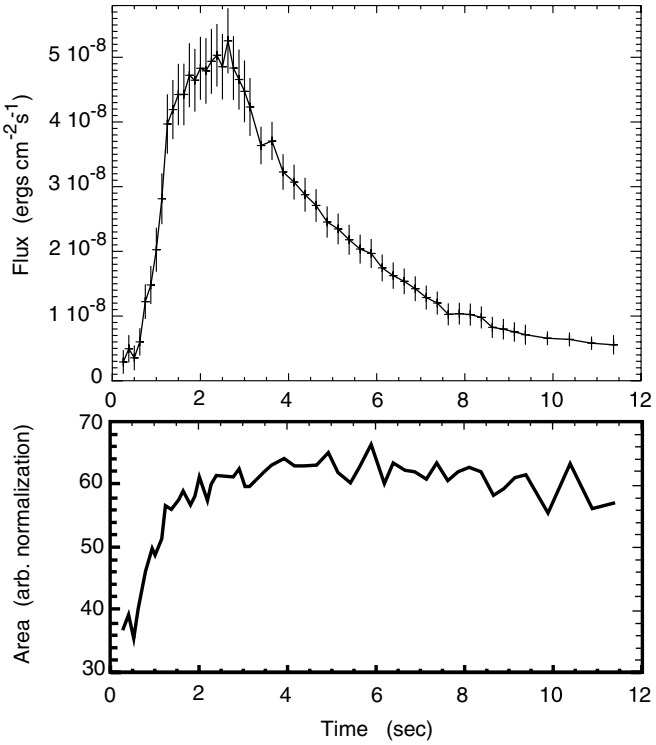

Figure 13. A thermonuclear x-ray burst from the neutron star in the low-mass x-ray binary system 4U 1728–34, as observed with the Rossi x-ray timing explorer. The top shows the rapid increase of the x-ray flux, followed by a slower decay. The lower panel indicates the change of the x-ray emitting area calculated for blackbody radiation from a specical system. The initial increase of the area provides strong evidence of the spread of the nuclear burning front over the entire surface of the neutron star (courtesy: Tod Strohmayer).

8.3. X-ray bursts

At present x-ray bursts are explained as thermonuclear runaways in the hydrogen-rich envelope of an accreting neutron star [159, 160]. Figure 13 shows the observed light curve of a single x-ray burst, which rapidly increases within seconds to maximum intensity. Low accretion rates favour a sudden local ignition of the material with a subsequent rapid spread over the neutron star surface [161]. This is also indicated in figure 13 which shows the spreading of the burning front over the entire neutron star surface.

The thermonuclear runaway is triggered by the ignition of the triple-alpha reaction and the break-out reactions from the hot CNO cycles [151]. Therefore the onset of the x-ray burst critically depends on the rates of the alpha-capture reactions on ^{15}O and ^{18}Ne. Figure 14 shows the predicted x-ray burst luminosity calculated using the currently suggested reaction rates which are based on strong resonance contributions in the low-energy range [162, 163]. Also shown in comparison is the luminosity calculated for the experimental minimum for the two reaction rates [162, 164] which do not take into account the anticipated low-energy contributions. This reduces the reaction rate by up to approximately five orders of magnitude in the temperature range of the hot CNO cycles.

Using the experimental minimum for the break-out reaction rates, a broad burst is observed, which is predominantly fuelled by the hot CNO cycles and the feeding triple-alpha process.

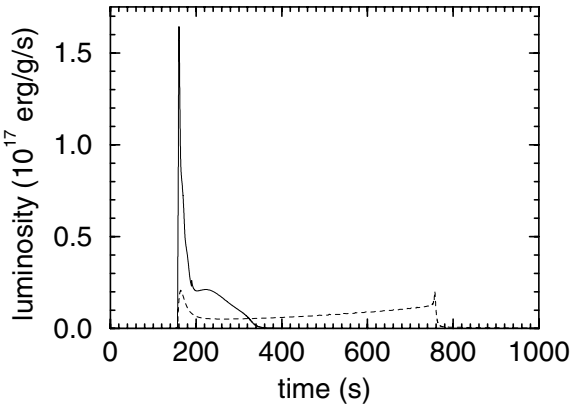

Figure 14. The predicted luminosity produced by nuclear reactions in the accreted envelope of a neutron star. The solid curve shows the expected luminosity including both break-out reactions ^{18}Ne(α, p)^{21}Na and ^{15}O(α, γ)^{19}Ne; the dotted curve shows the luminosity for break-out reactions with rates reduced by more than five orders of magnitude.

After an initial rapid increase the burst lasts for $\approx$ 500 s at a very slowly increasing luminosity, before rapidly decaying due to helium depletion. The afterglow is due to the decay of the enriched ^{14}O, ^{15}O, and ^{18}Ne abundances. This luminosity curve differs substantially from observed x-ray burst light curves. Including the low-energy contributions to the break-out reaction rates results in an entirely different luminosity structure, a rapid increase to an order of magnitude higher luminosity followed by a decline over a 100 s timescale. This is due to the rapid processing of the CNO material towards ^{56}Ni in the first few seconds of the thermonuclear runaway.

This thermonuclear runaway itself is driven by the αp-process and the rapid proton process (short rp-process), which convert the initial material rapidly to ^{56}Ni, causing the formation of Ni oceans at the neutron star surface. The αp-process is characterized by a sequence of (α, p) and (p, γ) reactions processing the ashes of the hot CNO cycles ^{14}O and ^{18}Ne up to the ^{34}Ar and ^{38}Ca range. The rp-process represents a sequence of rapid proton captures up to the proton drip-line and subsequent β-decays of drip-line nuclei processing the material from the argon–calcium range up to ^{56}Ni and beyond (see figure 15). The runaway freezes out in thermal equilibrium at peak temperatures of around 2.0–3.0 billion K. Re-ignition takes place during the subsequent cooling phase of the explosion via the rp-process beyond ^{56}Ni. The nucleosynthesis in the cooling phase of the burst alters considerably the abundance distribution in the atmosphere, ocean and subsequently crust of the neutron star. This may have a significant impact on the thermal structure of the neutron star surface and on the evolution of oscillations in the oceans [165, 166].

To verify the present models nuclear reaction and structure studies on the neutron-deficient side of the line of stability are essential [167]. Measurements of the break-out reactions will set stringent limits on the ignition conditions for the thermonuclear runaway; measurements of alpha and proton capture on neutron-deficient radioactive nuclei below ^{56}Ni will set limits on the timescale for the actual runaway but will also affect other macroscopic observables. Recent simulations of the x-ray burst characteristics with self-consistent multi-zone models suggested a significant impact of proton capture reaction rates between $A = 20$ and 64 on expansion velocity, temperature and luminosity of the burst [156, 168]. Indeed, the currently suggested reaction rates carry enormous uncertainties [167, 169, 170]. Recent use of the nuclear shell

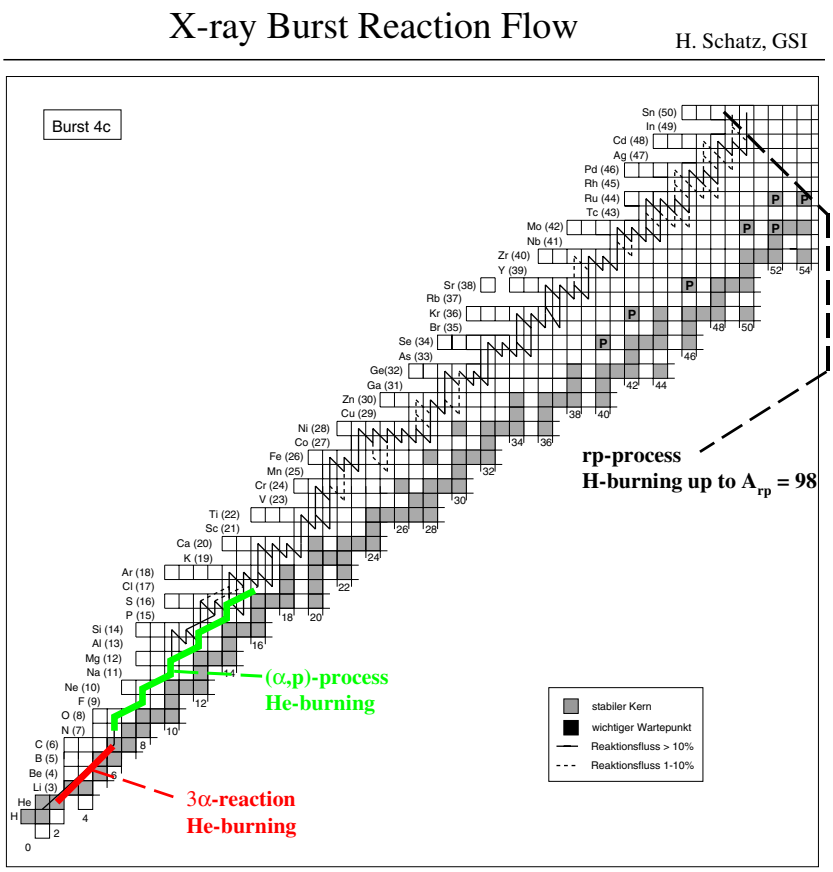

Figure 15. *Rp*-process reaction flow pattern in a typical x-ray burst simulation [167].

model [171, 172] to calculate proton capture reactions in this mass range more reliably did indeed indicate up to several orders of magnitude discrepancies in the global Hauser–Feshbach predictions [167]. Figure 16 shows for several reactions a comparison between some of the currently available predictions to elucidate the range of uncertainty in many of the reaction rates. Clearly, more experimental data are necessary to remove the present uncertainties.

Nuclear structure and nuclear reaction measurements near the double-closed-shell nucleus ^{56}Ni determine the conditions for the re-ignition of the burst in its cooling phase. Structure and reaction measurements beyond ^{56}Ni, in particular the experimental study of two-proton capture reactions bridging the drip-line for even–even $N = Z$ nuclei such as ^{68}Se and ^{72}Kr are necessary to determine the final fate of the neutron star crust. These reaction measurements have to be complemented with decay studies. Of particular importance are beta-decay studies of isomeric and/or thermally populated excited states, which are not accessible for experiment with present equipment. In general there is a substantial need for nuclear structure information at the proton drip-line, especially in the Ge–Kr mass region [173]. The information needed to calculate the flow of nuclear reactions in x-ray bursts includes masses, lifetimes, level structures and proton separation energies.

An important question is that for the endpoint of the *rp*-process. The endpoint is determined both by the macroscopic timescale of the burst, which depends on the various

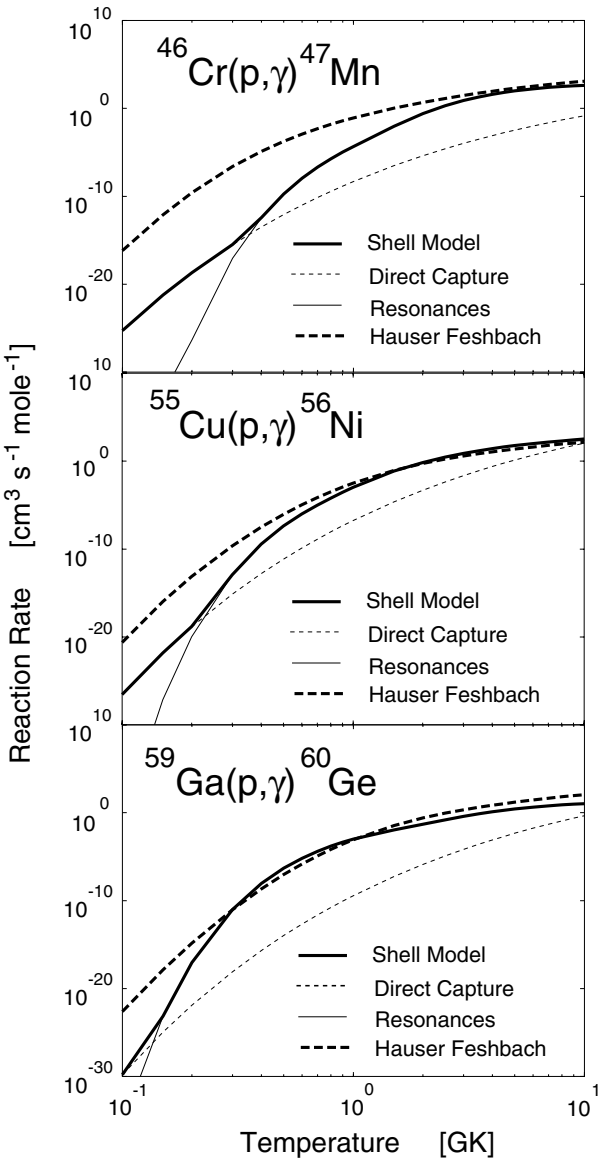

Figure 16. Reaction rates for proton capture reactions near the proton drip-line, ^{46}Cr(p, γ)^{47}Mn, ^{55}Cu(p, γ)^{56}Zn and ^{59}Ga(p, γ)^{60}Ge, at temperatures relevant for explosive hydrogen burning. The shell-model rates (solid curves) are compared with the Hauser–Feshbach estimate of [167] (dashed curves). In addition we show the resonant (fine solid) and direct-capture (dotted curves) contributions to the shell-model rates. There is a distinct discrepancy between these predictions. For these cases the Hauser–Feshbach approach is handicapped due to the low level density in the associated nuclei. The direct capture plays a dominant role in all three cases.

cooling mechanisms, and the microscopic timescale, given by the effective lifetimes of the waiting point nuclei along the reaction path. For steady-state burning scenarios, characterized by long-term high-temperature conditions, the endpoint is basically determined by the availability of hydrogen fuel in the accreted layer. All of the predicted reaction and decay rates

along the reaction path need to be experimentally tested and verified, yet the present predictions suggest a reaction flow even beyond ^{100}Sn [167, 174]. This raises the question of the actual endpoint. Alpha-decay studies in the mass range above ^{100}Sn suggest that the neutron-deficient isotopes ^{106}Te–^{108}Te and ^{108}I predominantly decay into the α-channel [175]. The isotope ^{109}I has been identified as a short-lived proton emitter [176]. These observations suggest that the actual endpoint of the rp-process might be associated with rapid backprocessing of the material via ^{104}Sb(p,α)^{101}Sn, ^{105}Sb(p, α)^{102}Sn and possibly also ^{106}Sb(p, α)^{103}Sn. While some mass models [177, 178] predict ^{104}Sb and ^{105}Sb to be proton unbound, the experimental decay rates are longer than Hauser–Feshbach predictions for the (p, α) reaction rates. Only a small amount of ^{106}Te, ^{107}Te is produced by ^{105}Sb(p, γ) and ^{106}Sb(p, γ), respectively and will be rapidly depleted by ^{106}Te(p, α)^{103}Sb and ^{107}Te(p, α)^{104}Sb. Detailed reaction flow calculations for the rp-process have been performed to simulate the reaction flow in this mass range. It was clearly shown that multi-cycling emerges in the Sn–Te–I range. This cycle presents a strong impedance for the rp-process and has been identified as the actual end-point for the reaction path [179].

8.4. X-ray pulsars

X-ray pulsars are interpreted as accreting neutron stars with high accretion rates and large magnetic fields, which funnel the accreted material to the pole cap thus reaching local accretion rates [180]. This causes a steady burning of the accreted material via the αp- and rp-processes on the surface of the neutron star. Detailed studies of the nucleosynthesis suggest that the accreted material is rapidly converted to heavier elements in the 80–100 mass range, which changes drastically the composition of the crust and the ocean of the neutron star, replacing the original iron crust by a mixture of significantly more massive elements. Thus the composition of the neutron star crust in a binary system is substantially different from that in a primordial single neutron star. This may have important effects on the thermal and electromagnetic conditions at the neutron star surface. The modified mass composition may also affect the observed decay of the magnetic field of the neutron star and its rotational r-modes due to shear effects.

The final composition depends strongly on the nuclear physics associated with the rp-process and the endpoint of the rp-process, which is directly correlated with the accretion rate. For experimental confirmation in the lower mass range, studies similar to those for the x-ray burst simulations are required [181]. However, for accretion in excess of 50 times the Eddington limit the endpoint of the rp-process is expected to lie in the 150 mass range. This requires a new range of nuclear structure data near the limits of stability. Of particular interest are beta-decay lifetimes, and especially processes such as beta-delayed proton and beta-delayed alpha-decays. If these processes dominate, as is expected for the decay of very neutron-deficient tellurium, iodine and xenon isotopes, a natural halting point for the rp-process is reached [179].

8.5. Black hole and neutron star accretion discs

Many of the accretion processes on neutron stars and black holes take place through accretion discs. Therefore it is necessary to investigate nuclear interaction processes that may occur during the accretion process at the local accretion disc in low-density and high-temperature conditions. Such processes may be of relevance for modelling x-ray bursts and x-ray pulsar events since such processes may alter the abundance distribution of the accreted material substantially [182]. At the fairly high-temperature conditions of an accretion disc a considerable amount of the accreted hydrogen may actually be consumed before entering

the neutron star atmosphere. This may affect our current understanding of the nucleosynthesis and energy release following ignition of the accreted material in thermonuclear runaways or steady burning modes. On the other hand interaction of the high-velocity accreted material with the outer atmospheres of the accreting object may cause spallation and fragmentation of the accreted material, which in turn may greatly alter its composition and regenerate part of the pre-consumed hydrogen [183]. Clearly detailed nucleosynthesis studies in the accretion disc and during impact on the outer atmosphere of a neutron star are necessary to address these problems.

9. Nucleosynthesis and cosmic rays

Galactic cosmic rays are charged particles from beyond the solar system accelerated to very high energies [184]. The origin of the cosmic rays is still under debate but a consensus seems to emerge that the production site is associated with the shockwaves of a supernova interacting with the stellar medium [185]. The dominant component of the cosmic rays is the stripped nuclei of atoms. Detailed measurements of cosmic ray composition are normally made at energies of a few hundred MeV u^{-1}. Cosmic rays are confined in the galaxy by galactic magnetic fields and so propagate through the ISM.

Determinations of cosmic ray source composition provide an opportunity for observational tests of galactic nucleosynthesis calculations. Galactic cosmic ray nuclei constitute a unique sample of material from outside the solar system. From measurements of cosmic ray secondary radio-nuclides it is known that cosmic rays are $10^{5(7)}$ years old. Thus, cosmic rays are relatively contemporary when contrasted with solar system material, which is evolution since the solar system formed. Measurements of the source composition also constrain theories as to the exact origin of the cosmic rays [185].

Cosmic ray composition is closely correlated with nuclear physics. While the source composition of cosmic rays constrains models of nucleosynthesis, nuclear physics is required to determine that source composition from actual measurements. Cosmic rays are also unique in being a relatively contemporary sample of galactic material where the isotopic composition can be measured up through the isotopes of Ni, and potentially beyond.

The elemental composition of cosmic rays deviates considerably from standard solar system abundances. For the more abundant elements, such as C, O, Ne, Mg, Si and Fe, the cosmic ray abundances approximate solar system abundances. For the rarer isotopes, such as Li, Be, B, Sc, V and Cr, the cosmic rays show huge enhancements. This is understood to be a result of nuclear spallation of the cosmic rays as they pass through the material of the ISM. The spallation processes produce the secondary components in the cosmic ray abundance distribution. Spallation reactions apply equally to isotopes; the rarer carbon and oxygen isotopes (^{13}C and ^{17}O, ^{18}O) therefore have large secondary components.

Once the secondary contribution is understood, it is possible to determine a primary, or source, composition of the cosmic rays in the framework of a cosmic ray propagation model. Any interpretation of these data must rely critically on a knowledge of the physics of nuclear spallation. For many critical isotopes, our knowledge of nuclear physics currently falls short of the precision of newly available cosmic ray data.

10. Conclusion

In the last 50 years our understanding of the abundances and the sources of the elements in the observable universe has grown into a mature and important science, generally referred to as nuclear astrophysics. It is a truly interdisciplanary field, combining astrophysics and nuclear physics with observational astronomy, and concentrates on primordial and stellar

nucleosynthesis, stellar evolution, and the interpretation of cataclysmic stellar events such as novae and supernovae. It is quite a scientific achievement that one now understands the relative abundances of most elements in our solar system and is able to reproduce them in evolutionary models of our galaxy with an accuracy of usually better than a factor of two.

Nuclear astrophysics has been and will be tremendously stimulated by recent developments in laboratory and observational techniques. In the laboratory, the planning and development of radioactive ion beam facilities as well as low-energy underground facilities promise to remove the most crucial ambiguities in nuclear astrophysics arising from nuclear physics input parameters. This progress goes hand in hand with decisive developments in astronomical observation. New spectroscopic capabilities have become available on the Hubble space telescope, and new large telescope facilities are now available through the VLT, the Keck and the new technology telescope at ESO. The most recent and rapid increase in observational data from satellite observations of intense galactic gamma-sources, observation and analysis of isotopic and elemental abundances in deep convective red giant and asymptotic giant branch stars and abundance and dynamical studies of nova ejecta and supernova remnants, as well as the large number of recently initiated and proposed experiments for measuring the solar and supernova neutrino flux, allow the placement of stringent limits on the various stellar and nucleosynthesis models. Also, the latest developments in modelling stars, novae, x-ray bursts and type I supernovae allow now much better predictions from nucleosynthesis calculations to be compared with the observational data.

Acknowledgments

We would like to thank our long-term collaborators Gabriel Martínez-Pinedo and Hendrik Schatz, who have contributed significantly to some of the work discussed in this review. Our research has been supported in part by grants from the Danish Research Council and the National Science Foundation.

References

[1] Burbidge E M, Burbidge G R, Fowler W A and Hoyle F 1957 *Rev. Mod. Phys.* **29** 547
[2] Anders E and Grevesse N 1989 *Geochim. Cosmochim. Acta* **53** 197
[3] Weinberg S 1972 *Gravitation and Cosmology* (New York: Wiley)
[4] Kolb E W and Turner M S 1990 *The Early Universe* (Reading, MA: Addison-Wesley)
[5] Smith M S, Kawano L H and Malaney R A 1993 *Astrophys. J.* **85** 219
[6] Riess A G *et al* 1998 *Astrophys. J.* **116** 1009
[7] Perlmutter S *et al* 1999 *Astrophys. J.* **517** 565
[8] Netterfield C B *et al* 2001 *Preprint* astro-ph/0104460
[9] Wallerstein G *et al* 1997 *Rev. Mod. Phys.* **69** 995
[10] Chieffi A, Limongi M and Straniero O 1998 *Astrophys. J.* **502** 737
[11] Adelberger E G *et al* 1998 *Rev. Mod. Phys.* **70** 1265
[12] Kunz R, Jaeger M, Mayer A, Hammer J W, Staudt G, Harissopulos S and Paradellis T 2001 *Phys. Rev. Lett.* **86** 3244
[13] Brune C R *et al* 2001 *Nucl. Phys.* A **688** 263c
[14] Buchmann L *et al* 2001 *Nucl. Phys.* A **688** 259c
[15] Görres J *et al* 2001 *Phys. Rev.* C **62** 055801
[16] Rauscher T, Thielemann F K, Görres J and Wiescher M 2000 *Nucl. Phys.* A **675** 695
[17] Pinsonneault M 1997 *Annu. Rev. Astron. Astrophys.* **35** 557
[18] Smith V V and Lambert D L 1990 *Astrophys. J. Suppl.* **72** 387
[19] Merrill P W 1952 *Science* **115** 484
[20] Zinner E 1998 *Annu. Rev. Earth Planet. Sci.* **26** 147
[21] Käppeler F, Beer H and Wisshak K 1989 *Rep. Prog. Phys.* **51** 949

[22] Meyer B S 1994 *Annu. Rev. Astron. Astrophys.* **32** 153
[23] Käppeler F *et al* 1990 *Astrophys. J.* **354** 630
[24] Käppeler F *et al* 1994 *Astrophys. J.* **437** 396
[25] Busso M, Gallino R and Waserburg G J 1999 *Annu. Rev. Astron. Astrophys.* **37** 239
[26] Bao Z Y, Beer H, Käppeler F, Voss F, Wisshak K and Rauscher T 2000 *At. Data Nucl. Data Tables* **76** 70
[27] Gallino R *et al* 1998 *Astrophys. J.* **487** 388
[28] Sneden C 2001 *Nature* **409** 673
[29] Hix R, Khoklov A M, Wheeler J C and Thielemann F-K 1998 *Astrophys. J.* **503** 332
[30] Tsujimoto T, Nomoto K, Yoshii Y, Hashimoto M and Thielemann F-K 1995 *Mon. Not. R. Astron. Soc.* **277** 945
[31] Bethe H A 1990 *Rev. Mod. Phys.* **62** 801
[32] Bethe H A, Brown G E, Applegate J and Lattimer J M 1979 *Nucl. Phys.* A **324** 487
[33] Goldreich P and Weber S V 1980 *Astrophys. J.* **238** 991
[34] Burrows A 1990 *Annu. Rev. Nucl. Sci.* **40** 181
[35] Burrows A 1988 *Astrophys. J.* **334** 891
[36] Wilson J R 1985 *Numerical Astrophysics* ed J M Centrella, J M LeBlanc and R L Bowers (Boston: Jones and Bartlett) p 422
[37] Mezzacappa A 2001 *Nucl. Phys.* A **688** 158c
[38] Janka H-T and Rampp M 2000 *Astrophys. J.* **539** L33
[39] Woosley S E and Weaver T A 1995 *Astrophys. J. Suppl.* **101** 181
[40] Thielemann F-K, Nomoto K and Hashimoto M 1996 *Astrophys. J.* **460** 408
[41] Fuller G M, Fowler W A and Newman M J 1980 *Astrophys. J. Suppl.* **42** 447
Fuller G M, Fowler W A and Newman M J 1982 *Astrophys. J. Suppl.* **48** 279
Fuller G M, Fowler W A and Newman M J 1982 *Astrophys. J.* **252** 715
[42] Brown B A and Wildenthal B H 1988 *Ann. Rev. Nucl. Part. Sci.* **38** 29
[43] Caurier E 1989 ANTOINE, computer code, CRN Strasbourg
[44] Caurier E, Langanke K, Martinez-Pinedo G and Nowacki F 1999 *Nucl. Phys.* A **653** 439
[45] Langanke K and Martinez-Pinedo G 2000 *Nucl. Phys.* A **673** 481
[46] Heger A, Langanke K, Martinez-Pinedo G and Woosley S E 2001 *Phys. Rev. Lett.* **86** 1678
[47] Heger A, Woosley S E, Martinez-Pinedo G and Langanke K *Astrophys. J.* at press
[48] Oda T, Hino M, Muto K, Takahara M and Sato K 1994 *At. Data Nucl. Data Tables* **56** 231
[49] Mazurek T 1966 *PhD Thesis* Yale University
[50] Aufderheide M B, Fushiki I, Fuller G M and Weaver T A 1994 *Astrophys. J.* **424** 257
[51] Mezzacappa A 2001 Private communication
[52] Mezzacappa A and Bruenn S W 1993 *Astrophys. J.* **405** 669
[53] Keil W, Janka H-T and Müller E 1996 *Astrophys. J. Lett.* **473** L111
[54] Bruenn S W 1985 *Astrophys. J. Suppl.* **58** 771
[55] Cooperstein J and Wambach J 1984 *Nucl. Phys.* A **420** 591
[56] Langanke K, Kolbe E and Dean D J 2001 *Phys. Rev.* C **63** 032801
[57] Johnson C W, Koonin S E, Lang G H and Ormand W E 1992 *Phys. Rev. Lett.* **69** 3157
Koonin S E, Dean D J and Langanke K 1997 *Phys. Rep.* **278** 1
[58] Langanke K, Martinez-Pinedo G and Sampaio J M 2001 *Phys. Rev.* C **64** 055801
[59] Haxton W C 1988 *Phys. Rev. Lett.* **60** 1999
[60] Bruenn S W and Haxton W C 1991 *Astrophys. J.* **376** 678
[61] Toivanen J, Kolbe E, Langanke K, Martinez-Pinedo G and Vogel P 2001 *Nucl. Phys.* A 694 **395**
[62] Woosley S E, Hartmann D, Hoffman R D and Haxton W C 1990 *Astron. J.* **356** 272
[63] Sampaio J M, Langanke K and Martinez-Pinedo G 2001 *Phys. Lett.* B 511 **11**
[64] Sampaio J M, Langanke K and Martinez-Pinedo G unpublished
[65] Sawyer R F 1989 *Phys. Rev.* C **40** 865
[66] Reddy S, Prakash M, Lattimer J M and Pons S A 1999 *Phys. Rev.* C **59** 2888
[67] Reddy S, Prakash M and Lattimer J M 1998 *Phys. Rev.* D **58** 3009
[68] Burrows A and Sawyer R F 1998 *Phys. Rev.* C **58** 554
[69] Burrows A and Sawyer R F 1999 *Phys. Rev.* C **59** 510
[70] Margueron J, Navarro J, Jiang W and Van Giai N 2001 *The Nuclear Many-Body Problem* ed D Vretenar and W Nazarewicz (Dordrecht: Kluwer)
[71] Janka H-T and Müller E 1996 *Astron. Astrophys.* **306** 167
[72] Müller E and Janka H-T 1997 *Astron. Astrophys.* **317** 140
[73] Burrows A and Fryxell B A 1992 *Science* **258** 430
[74] Wilson J R and Mayle R W 1993 *Phys. Rep.* **227** 97

[75] Bruenn S W and Dineva T 1996 *Astrophys. Lett.* **458** L71
[76] Thompson T A and Burrows A 2001 *Nucl. Phys.* A **688** 377c
[77] Mezzacappa A *et al* 1998 *Astron. J.* **493** 848
[78] Herant M *et al* 1994 *Astron. J.* **435** 339
[79] Burrows A, Hayes J and Fryxell B A 1995 *Astrophys. J.* **450** 830
[80] Cameron A G W 1957 *Chalk River Report* CRL–41
[81] Kratz K L *et al* 1993 *Astrophys. J.* **402** 216
[82] Möller P, Nix J R and Kratz K L 1997 *At. Data Nucl. Data Tables* **66** 131
[83] Borsov I N, Goriely S and Pearson J M 1997 *Nucl. Phys.* A **621** 307c
[84] Demetriou P and Goriely S 2001 *Nucl. Phys.* A **688** 584c
[85] Dobaczewski J *et al* 1994 *Phys. Rev. Lett.* **72** 981
[86] Chen B *et al* 1995 *Phys. Lett.* B **355** 37
[87] Pfeiffer B, Kratz K L and Thielemann F K 1997 *Z. Phys.* A **357** 235
[88] Kratz K-L, Görres J, Pfeiffer B and Wiescher M 2000 *J. Radioanal. Nucl. Chem.* **243** 133
[89] Kratz K-L, Möller P, Pfeiffer B and Walters W B 2000 *Capture Gamma-Rays and Related Studies (AIP Conf. Proc. vol 529)* ed S Wender p 295
[90] Kratz K L 2001 *Nucl. Phys.* A **688** 308c
[91] Sharma M M and Farhan A R 2001 *Nucl. Phys.* A **688** 353c
[92] Surman R, Engel J, Bennett J R and Meyer B S 1997 *Phys. Rev. Lett.* **79** 1809
[93] Kratz K L *et al* 1988 *J. Phys. G: Nucl. Phys.* **24** S331
[94] Kratz K L *et al* 1986 *Z. Phys.* A **325** 489
[95] Lettry J *et al* 1998 *Rev. Sci. Instrum.* **69** 761
[96] Engel J *et al* 1999 *Phys. Rev.* C **60** 014302
[97] Martinez-Pinedo G and Langanke K 1999 *Phys. Rev. Lett.* **83** 4502
[98] Martinez-Pinedo G 2001 *Nucl. Phys.* A **688** 57c
[99] Rauscher T, Thielemann F-K and Kratz K L 1997 *Phys. Rev.* C **56** 1613
[100] Cowan J J, Thielemann F-K and Truran J W 1991 *Phys. Rep.* **208** 267
[101] Nakada H and Alhassid Y 1997 *Phys. Rev. Lett.* **79** 2939
[102] Langanke K 1998 *Phys. Lett.* B **438** 235a
[103] Alhassid Y, Bertsch G F, Liu S and Nakada H 2000 *Phys. Rev. Lett.* **84** 4313
[104] Gurevich G M *et al* 1981 *Nucl. Phys.* A **351** 257
[105] Catara F, Lanzo E G, Nagarajan M A and Vitturi A 1997 *Nucl. Phys.* A **624** 449
[106] Vretenar D, Paar N, Ring P and Lalazissis G *Nucl. Phys.* A at press
[107] Goriely S 1998 *Phys. Lett.* **436** 10
[108] Sneden C *et al* 2000 *Astrophys. J.* **533** L139
[109] Goriely S and Arnould M 1997 *Astron. Astrophys.* **322** L29
[110] Wasserburg G J, Busso M and Gallino R 1996 *Astrophys. J.* **466** L109
[111] Qian Y-Z, Vogel P and Wasserburg G J 1998 *Astrophys. J.* **494** 285
[112] Woosley S E, Wilson J R, Mathews G J, Hoffmann R D and Meyer B S 1994 *Astrophys. J.* **433** 229
[113] Witti J, Janka H-Th and Takahashi K 1994 *Astron. Astrophys.* **286** 841
Witti J, Janka H-Th and Takahashi K 1994 *Astron. Astrophys.* **286** 857
[114] Truran J W, Cowan J J and Field B D 2001 *Nucl. Phys.* A **688** 330c
[115] Freiburghaus C, Rosswog S and Thielemann F K 1999 *Astrophys. J.* **525** L121
[116] Rosswog S, Davies M B, Thielemann F K and Piran T 2000 *Astron. Astrophys.* **360** 171
[117] Thielemann F-K, Rauscher T, Freiburghaus C, Nomoto K, Hashimoto M, Pfeiffer B and Kratz K-L at press
[118] Qian Y-Z 1997 *Nucl. Phys.* A **621** 363c
Qian Y-Z and Woosley S E 1996 *Astrophys. J.* **471** 331
[119] Meyer B S, Mathews G J, Howard W M, Woosley S E and Hoffman R D 1992 *Astrophys. J.* **399** 656
[120] Qian Y-Z and Woosley S E 1996 *Astrophys. J.* **471** 331
[121] Hofmann R D, Woosley S E and Qian Y-Z 1997 *Astrophys. J.* **482** 951.
[122] Qian Y-Z and Fuller G M 1995 *Phys. Rev.* D **52** 656
Qian Y-Z 1997 *Nucl. Phys.* A **621** 363c
[123] Fuller G M 2001 *Nucl. Phys.* A **688** 322c
[124] Meyer B S, McLaughlin G C and Fuller G M 1998 *Phys. Rev.* C **58** 3696
[125] Sumiyoshi K *et al* 2001 *Nucl. Phys.* A **688** 478c
[126] McLaughlin G C and Fuller G M 1997 *Astrophys. J.* **489** 768
[127] Qian Y-Z, Haxton W C, Langanke K and Vogel P 1997 *Phys. Rev.* C **55** 1532
[128] Hektor A, Kolbe E, Langanke K and Toivanen J 2000 *Phys. Rev.* C **61** 055803

[129] Haxton W C, Langanke K, Qian Y-Z and Vogel P 1997 *Phys. Rev. Lett.* **78** 2694
[130] Fuller G M and Meyer B S 1995 *Astrophys. J.* **453** 792
[131] McLaughlin G C and Fuller G M 1995 *Astrophys. J.* **455** 202
[132] Terasawa M *et al* 2001 *Nucl. Phys.* A **688** 581c
[133] Langanke K and Kolbe E *At. Data Nucl. Data Tables* at press
[134] Woosley S E *et al* 1990 *Astrophys. J.* **356** 272
[135] Timmes F, Woosley S E and Weaver T A 1995 *Astrophys. J. Suppl.* **98** 617
[136] Haxton W C 2000 *Preprint* nucl-th/0012063
[137] von Neumann-Cosel P *et al* at press
[138] De Belic *et al* 1999 *Phys. Rev. Lett.* **83** 5242
[139] Arnould M 1998 *Proc. Hirschegg Conf. on Nuclear Astrophysics* ed M Buballa, W Nörenberg, J Wambach and A Wirzba (GSI)
[140] Cayrel R *et al* 2001 *Nature* **409** 691
[141] Cowan J J *et al* 1999 *Astrophys. J.* **521** 194
[142] Goriely S and Clerbaux B 1999 *Astron. Astrophys.* **346** 804
[143] Clayton D D 1964 *Astrophys. J.* **139** 637
[144] Winters R R, Maklin R L and Halperin J 1980 *Phys. Rev.* C **21** 563
Winters R R and Maklin R L 1982 *Phys. Rev.* C **25** 208
[145] Bosch F *et al* 1996 *Phys. Rev. Lett.* **77** 5190
[146] Fryxell B *et al* 2001 *Nucl. Phys.* A **688** 172c
[147] Truran J W 1982 *Essays in Nuclear Astrophysics* ed C A Barnes, D D Clayton and D N Schramm (Cambridge: Cambridge University Press) p 467
[148] Glasner S A, Livne E and Truran J W 1997 *Astrophys. J.* **475** 754
[149] Shore S *et al* 1994 *Astrophys. J.* **421** 344
[150] Starrfield S, Truran J W, Wiescher M and Sparks W M 1998 *Mon. Not. R. Astron. Soc.* **296** 502
[151] Wiescher M, Görres J and Schatz H 1999 *J. Phys. G: Nucl. Part. Phys.* **25** R133
[152] Livio M and Truran J W 1994 *Astrophys. J.* **425** 797
[153] Starrfield S, Iliadis C, Truran J W, Wiescher M and Sparks W M 2001 *Nucl. Phys.* A **688** 110c
[154] Jose J, Coc A and Hernanz M 1999 *Astrophys. J.* **520** 347
[155] Prantzos N and Diehl R 1996 *Phys. Rep.* **267** 1
[156] Fisker J, Rembges F, Barnard V and Wiescher M 2001 *Proc. Workshop on the Influence of Binaries on Stellar Population Studies* (Dordrecht: Kluwer)
[157] Ruiz-Lapuente P, Canal R and Isern J 1997 *Thermonuclear Supernovae* (Dordrecht: Kluwer)
[158] Brachwitz F, Dean D J, Hix W R, Iwamoto K, Langanke K, Martínez-Pinedo G, Nomoto K, Strayer M R, Thielemann F-K and Umeda H 2000 *Astrophys. J.* **536** 934
[159] Taam R, Woosley S E, Weaver T and Lamb D 1993 *Astrophys. J.* **413** 324
[160] Lewin W H G, van Paradijs J and Taam R E 1993 *Space Sci. Rev.* **62** 233
[161] Bildsten L and Strohmayer T 1999 *Phys. Today* **52** 40
[162] Mao Z Q, Fortune H T and Lacaze A G 1996 *Phys. Rev.* C **53** 1197
[163] Görres J, Wiescher M and Thielemann F-K 1995 *Phys. Rev.* C **51** 392
[164] Bradfield-Smith W *et al* 1999 *Phys. Rev.* C **59** 3402
[165] Brown E 2000 *Astrophys. J.* **531** 988
[166] Bildsten L 1998 *Astrophys. J.* **501** L89
[167] Schatz H *et al* 1998 *Phys. Rep.* **294** 168
[168] Thielemann F-K *et al* 2001 *Prog. Part. Nucl. Phys.* **46** 5
[169] van Wormer L, Örres J, Iliadis C, Wiescher M and Thielemann F-K 1994 *Astrophys. J.* **432** 326
[170] Iliadis C, Endt P M, Prantzos N and Thompson W J 1999 *Astrophys. J.* **524** 434
[171] Herndl H, Görres J, Wiescher M, Brown B A and van Wormer L 1995 *Phys. Rev.* C **52** 1078
[172] Fisker J, Barnard V, Görres J, Langanke K, Martinez-Pinedo G and Wiescher M 2001 *At. Data Nucl. Data Tables* **79** 1
[173] Käppeler F, Thielemann F-K and Wiescher M 1998 *Annu. Rev. Nucl. Part. Sci.* **48** 175
[174] Wiescher M, Schatz H and Champagne A 1998 *Phil. Trans. R. Soc.* **356** 2105
[175] Page R D, Woods P J, Cunningham R A, Davinson T, Davis N J, James A N, Livingston K, Sellin P J and Shotter A C 1994 *Phys. Rev.* C **49** 3312
[176] Gillitzer A, Faestermann T, Hartel K, Kienle P and Nolte E 1987 *Z. Phys.* A **326** 107
[177] Möller P, Nix J R, Myers D and Swiatecki W J 1995 *At. Data Nucl. Data Tables* **59** 185
[178] Aboussir Y, Pearson J M, Dutta A K and Tondeur F 1992 *Nucl. Phys.* A **549** 155
[179] Schatz H *et al* 2001 *Phys. Rev. Lett.* **86** 3471

[180] Bildsten L and Brown E F 1997 *Astrophys. J.* **477** 897
[181] Schatz H, Bildsten L, Cummings A and Wiescher M 1999 *Astrophys. J.* **524** 1014
[182] Taam R E and Fryxell B A 1985 *Astrophys. J.* **294** 303
[183] Bildsten L, Salpeter E E and Wassermann I 1992 *Astrophys. J.* **384** 143
[184] Hillas A M 1984 *Annu. Rev. Astron. Astrophys.* **22** 425
[185] Biermann P L 1993 *Astron. Astrophys.* **271** 649